Geochemistry Geophysics Geosystems G3
AN ELECTRONIC JOURNAL OF THE EARTH SCIENCES
Published by AGU and the Geochemical Society

Research Letter
Volume 9, Number 4
30 April 2008
Q04039, doi:10.1029/2007GC001867
ISSN: 1525-2027

Evolving east Asian river systems reconstructed by trace element and Pb and Nd isotope variations in modern and ancient Red River-Song Hong sediments

Peter D. Clift
School of Geosciences, University of Aberdeen, Meston Building, Aberdeen AB24 3UE, United Kingdom (p.clift@abdn.ac.uk)

DFG-Research Centre Ocean Margins (RCOM) and Geowissenschaften (FB5), Universität Bremen, Klagenfurter Strasse, D-28359 Bremen, Germany

Hoang Van Long
School of Geosciences, University of Aberdeen, Meston Building, Aberdeen AB24 3UE, United Kingdom

Richard Hinton
Edinburgh Ion Microprobe Facility (EIMF), Department of Geology and Geophysics, University of Edinburgh, West Mains Road, Edinburgh EH9 3JW, United Kingdom

Robert M. Ellam
Scottish Universities Environmental Research Centre, Rankine Avenue, Glasgow G75 0QF, United Kingdom

Robyn Hannigan
Department of Chemistry and Physics, Arkansas State University, P.O. Box 1847, State University, Arkansas 72467, USA

Mai Thanh Tan
Hanoi University of Mining and Geology, Dong Ngac, Tu Liem, Hanoi, Vietnam

Jerzy Blusztajn
Department of Geology and Geophysics, Woods Hole Oceanographic Institution, Woods Hole, Massachusetts 02543, USA

Nguyen Anh Duc
Vietnam Petroleum Institute, Yen Hoa, Cau Giay, Hanoi, Vietnam

[1] Rivers in east Asia have been recognized as having unusual geometries, suggestive of drainage reorganization linked to Tibetan Plateau surface uplift. In this study we applied a series of major and trace element proxies, together with bulk Nd and single K-feldspar grain Pb isotope ion probe isotope analyses, to understand the sediment budget of the modern Red River. We also investigate how this may have evolved during the Cenozoic. We show that while most of the modern sediment is generated by physical erosion in the upper reaches in Yunnan there is significant additional flux from the Song Lo, draining Cathaysia and the SW Yangtze Block. Nd isotope data suggest that 40% of the modern delta sediment comes from the Song Lo. Carbonates in the Song Lo basin make this a major control on the Red River Sr budget. Erosion is not a simple function of monsoon precipitation. Active rock uplift is also required to drive strong erosion. Single grain Pb data show a connection in the Eocene between the middle Yangtze and the Red River, and probably with rivers draining the Songpan Garze terrane. However, the isotope data

do not support a former connection with the upper Yangtze, Mekong, or Salween rivers. Drainage capture appears to have occurred throughout the Cenozoic, consistent with surface uplift propagating gradually to the southeast. The middle Yangtze was lost from the Red River prior to 24 Ma, while the connection to the Songpan Garze was cut prior to 12 Ma. The Song Lo joined the Red River after 9 Ma. Bulk sample Pb analyses have limited provenance use compared to single grain data, and detailed provenance is only possible with a matrix of different proxies.

Components: 17,230 words, 16 figures, 5 tables.

Keywords: erosion; isotopes; provenance; rivers.

Index Terms: 1051 Geochemistry: Sedimentary geochemistry; 1039 Geochemistry: Alteration and weathering processes (3617); 9320 Geographic Location: Asia.

Received 24 October 2007; **Revised** 15 February 2008; **Accepted** 18 February 2008; **Published** 30 April 2008.

Clift, P. D., H. V. Long, R. Hinton, R. M. Ellam, R. Hannigan, M. T. Tan, J. Blusztajn, and N. A. Duc (2008), Evolving east Asian river systems reconstructed by trace element and Pb and Nd isotope variations in modern and ancient Red River-Song Hong sediments, *Geochem. Geophys. Geosyst.*, *9*, Q04039, doi:10.1029/2007GC001867.

1. Introduction

[2] Although links between changes in the Earth's climate and the tectonic evolution of the lithosphere have been suggested demonstration and quantification of these interactions has yet to be achieved. The uplift of the Tibetan Plateau and intensification of the Asian monsoon system is one of the most dramatic examples of such interactions acting on a continental scale [*Molnar et al.*, 1993; *Prell and Kutzbach*, 1992]. If such models are to be tested then independent records of uplift and climate change need to be reconstructed and compared. Constraining the paleoaltitude of Tibet is however difficult. Some progress has been made using improved paleobotanical methods [*Spicer et al.*, 2003], and in analyzing the oxygen isotope composition of soil carbonate and rainwater [*Garzione et al.*, 2000] in order to derive more quantitative estimates of limited areas of the plateau. Measuring widespread surface uplift is harder.

[3] However, regional surface uplift changes continental topographic gradients, which in turn influence the evolution of river systems in east Asia. In particular, it has been proposed that the Red River (Song Hong) was once the dominant river system in east Asia, and that much of its headwater drainage has been lost as a result of Cenozoic drainage reorganization driven by surface uplift in eastern Tibet [*Brookfield*, 1998; *Clark et al.*, 2004]. Such a process must affect the volume and compositions of sediments reaching the deltas in east Asia. Thus in theory we might use the sediment record from these deltas to date the timing of widespread uplift.

[4] In this paper we present a series of bulk sediment and single grain geochemical analyses from the modern Red River and from borehole samples from the Red River delta region (Hanoi Basin) in order to assess the degree of source heterogeneity in the modern river basin to pinpoint the source of the modern river sediment, and to see whether major changes in the drainage have occurred in the past. We attempt to resolve the different end-member sources that have supplied, and continue to supply sediment to the Red River. We build on the earlier bulk sediment work of *Liu et al.* [2007] by sampling the main trunk stream and both minor and major tributaries in order to assess their contributions to the total sediment flux. Each of the samples was analyzed for a series of major and trace elements, and for Sr and Nd isotopes where these data did not already exist. A subsection of the modern and ancient samples were then analyzed for Pb isotopes using both bulk sediment ICP-MS and by ion microprobe on single K-feldspar grains. These methods were chosen because of their proven effectiveness as provenance indicators in numerous modern and ancient catchments worldwide.

[5] *Clift et al.* [2006b] used thermochronological measurements from sand in the Red River delta to suggest that the bulk of the sand being carried by the modern river is eroded from those regions in the upper catchment, mostly in China now experiencing active rock uplift. This result is consistent with a mineralogical study of fine-grained sediments from along the course of the main Red River [*Liu et al.*, 2007]. These methods and our analyses

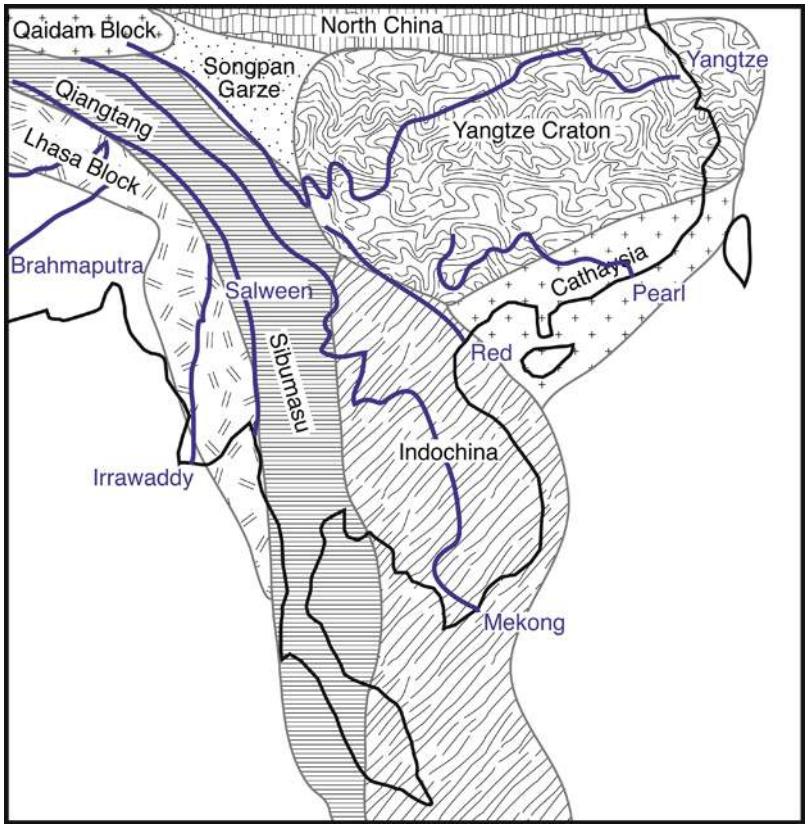

Figure 1. Simplified tectonic terrane map of east and Southeast Asia showing the major blocks discussed in this paper [*Metcalfe*, 1996] and the courses of the rivers colored in blue.

are based on the contrasting bedrock geology of SE Asia and eastern Tibet. Although much of the region was deformed during the Triassic Indosinian orogeny [*Carter et al.*, 2001; *Lepvrier et al.*, 2004] the region is composed of a series of continental blocks (Figure 1) whose chemical composition, as well as timing and intensity of metamorphism or magmatism differ. These differences are partially transferred to the river sediments, allowing the provenance of the sediment to be reconstructed if the appropriate tool is employed.

2. Drainage Capture from the Red River

[6] Evidence exists that the Red River has suffered major loss of headwater drainage. *Clark et al.* [2004] analyzed the nonsteady state drainage patterns in SE Asia to propose a major shift of headwater drainage away from the Red River. *Clift et al.* [2006a] estimated the volume of sediment in the Song Hong-Yinggehai Basins, located between Vietnam and Hainan Island in the South China Sea. These basins are fed by the Red River, but their volume is far in excess of what has been eroded onshore in the modern Red River drainage. These authors also used the Nd isotope system as a provenance tool to see how the river sediments changed through time. Bulk sediment compositions changed radically up-section throughout the Cenozoic, and achieved Nd isotope compositions close to that of the modern river by the Early Miocene, ~24 Ma.

[7] While this might suggest that headwater capture principally occurred during the Oligocene, there is evidence for continued capture in the form of significant Nd isotope variation since that time and a continued mismatch between eroded and deposited volumes of sediment. Although the direction of Nd isotope change is suggestive of loss of the middle Yangtze from the paleo-Red River during the Oligocene [*Clift et al.*, 2006a], this result is hard to verify because bulk sediment analysis necessarily results in an averaged provenance determination and does not allow the influence of minority sources to be constrained.

3. Analytical Strategy

[8] Both coarse and fine-grained lithologies were sampled at a series of river bed sites, mostly in

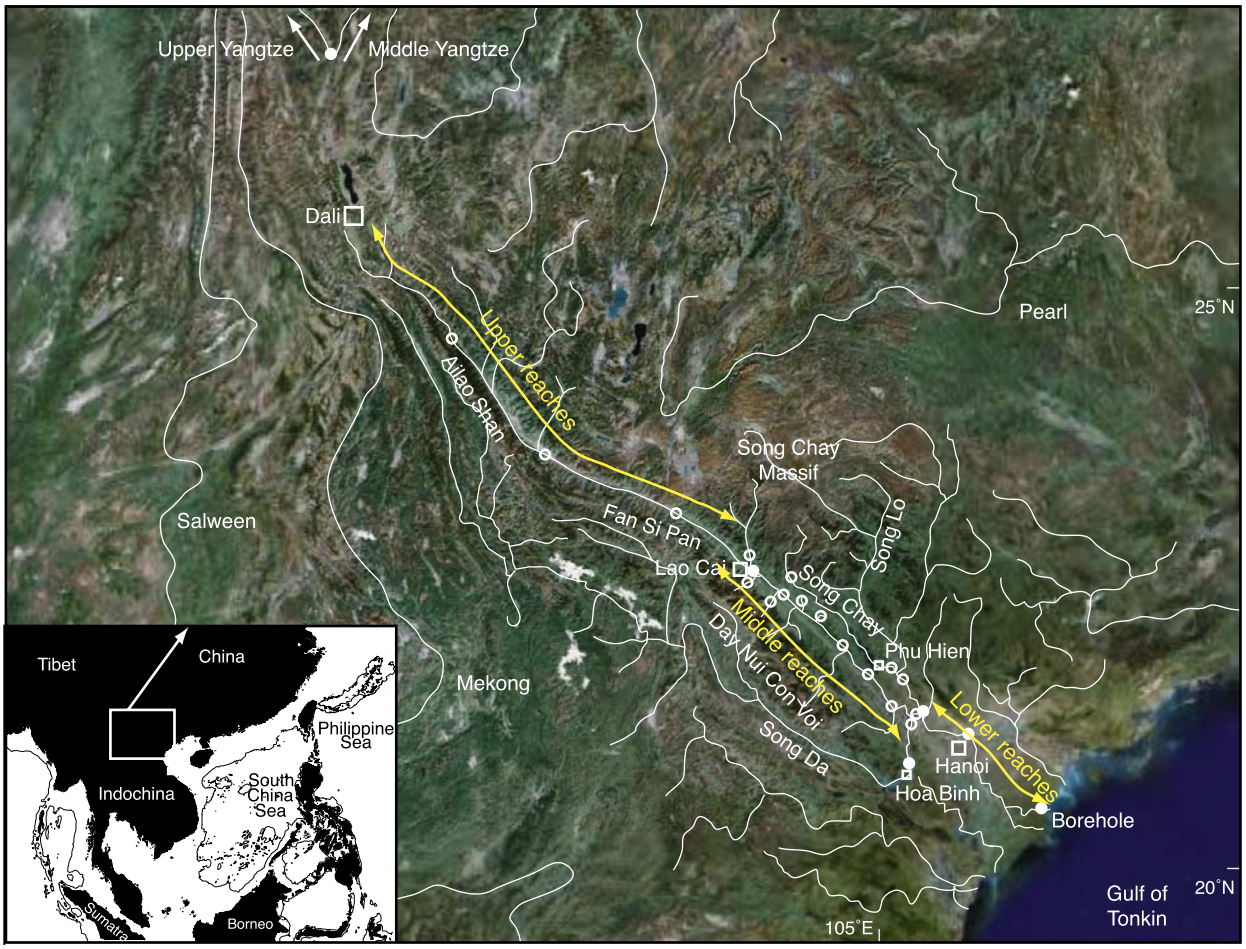

Figure 2. Satellite image of the Red River drainage basin showing the trunk river and the main tributaries as well as the course of the major neighboring rivers. White circles indicate the locations of samples taken for this study and analyzed for major and trace element compositions as well as Nd isotopes. White dots show samples also analyzed for Pb isotopes. Inset map shows location of image within east Asia.

Vietnam, but also from three locations in China, as well as at the ''first bend'' of the Yangtze (Figure 2). This first bend location is important because it samples those regions of Tibet eroded by the upper Yangtze and is proposed as a crucial capture point [*Clark et al.*, 2004], implying that this flux may have previously been delivered to a paleo-Red River. The Vietnamese samples were collected in May 2005 and the Chinese samples in May 2004, both prior to the onset of the summer monsoon. In Vietnam we target the Song Lo and Song Chay rivers, which erode basement largely associated with the Yangtze and Cathaysia blocks lying NE of the main river (Figures 1 and 3). We also collected materials from the Song Da, lying SW of the mainstream and eroding the northern parts of Indochina. The Song Da is disturbed by a major dam at Hoa Binh, installed 1979–1994, ~45 km from the confluence of the Song Da and Red River (Figure 2). Although the Song Chay is also dammed at Phu Hien this is considered less important because the Song Lo dominates this system below the Song Lo-Song Chay confluence. Finally a number of smaller rivers were collected close to their confluence with the Red River in order to characterize the chemical diversity of the local basement and to test the hypothesis that most of the sediment in the main river at Hanoi is derived from the tectonically active upper reaches.

[9] As well as modern river samples we sampled sedimentary rocks cored from a number of industrial boreholes located close together near the modern coast of the delta, and which were previously analyzed for Nd isotopes [*Clift et al.*, 2006a].

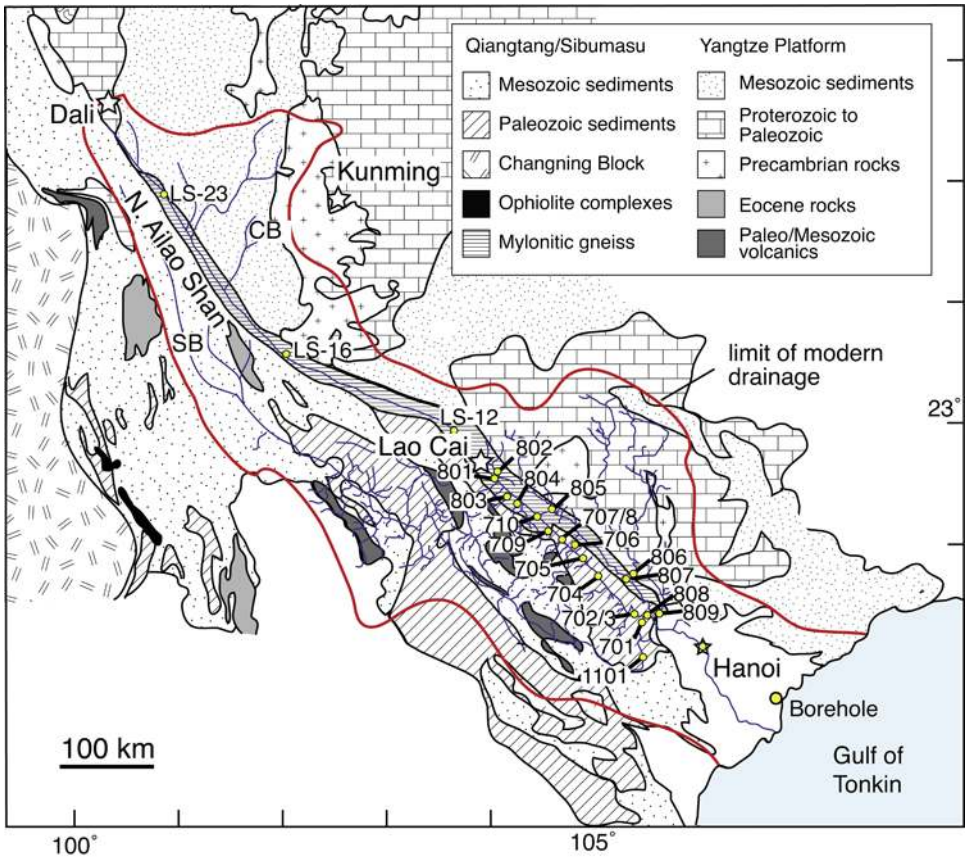

Figure 3. Regional geological map of the eastern Tibetan Plateau, SW China, and northern Indochina showing the river courses overlain in blue and the locations of sediment samples shown as yellow dots. Map redrawn from original provided by B. C. Burchfiel (unpublished data, 2006). CB, Chuxiong Basin; SB; Simao Basin.

Samples span the entire sedimentary section as deep as the Upper Eocene (Figure 4) and are relatively well dated by nannofossil biostratigraphy (confidential data from PetroVietnam). In addition, we use one sample from petroleum exploration well Wushi 22–3-1, located offshore (20°6.817′N, 109°11.610′E). In each case the depth to formation tops and bottoms are known, and these are defined at the sub-epoch level. We assign a numerical age to these horizons derived from the *Berggren et al.* [1995] timescale and assume a linear sedimentation rate between the dated horizons. In practice this means significant uncertainty in the numerical age but confidence in the order of the samples and the first-order temporal pattern. Together these samples provide an image of the changing erosional flux in the paleo-river. Because the Red River is confined to a canyon and has relatively small coastal floodplains it is unlikely that the lower reaches of the river were ever far from the modern delta region. Except for at the basin margins the fill of the onshore Hanoi and offshore Song Hong-Yinggehai Basins is considered to be supplied by the paleo-Red River, not local sources.

4. Analytical Methods

4.1. Bulk Major and Trace Element Analysis

[10] Major element analyses of bulk sediment samples were obtained by X-Ray Fluorescence at Franklin & Marshall College, Pennsylvania, using a Phillips 2404 XRF vacuum spectrometer. Working curves for each element of interest were determined by analyzing geochemical rock standards, data for which were synthesized by *Abbey* [1983] and *Govindaraju* [1994]. Between 30 and 50 data points are gathered for each working curve; various elemental interferences are also taken into account, e.g., SrKß on Zr, RbKß on Y. The Rh Compton peak was utilized for a mass absorption correction. Slope and intercept values, together with correction factors for the various wavelength interferences, were calculated.

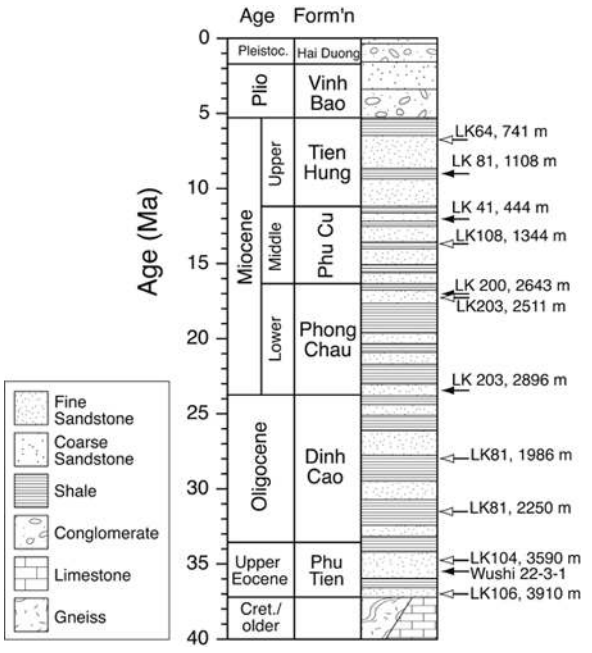

Figure 4. Sedimentary log of the drilled sequence in the Hanoi Basin showing the major stratigraphic divisions sampled during this study and their depositional ages. Black arrows indicate the locations of the samples selected for Pb isotope analysis by ion probe. White-headed arrows show the locations of samples analyzed for major and trace elements as well as for Nd isotopes by *Clift et al.* [2006a].

[11] The amount of ferrous Fe is titrated using a modified *Reichen and Fahey* [1962] method and loss on ignition was determined by heating an exact aliquot of the sample (1 g) at 950°C for one hour. The X-ray procedure determines the total Fe content as Fe_2O_3. Analytical errors associated with measuring major element concentrations range from <1% for Si and Al to ~3% for Na. The results of our analysis are shown in Table 1.

[12] Trace and rare earth elements (REE) were measured by a PerkinElmer Elan 9000 ICP-MS at Arkansas State University. Analytical precision is typically <2% of the reported concentrations of the individual elements. Uncertainty of the analyses, as determined from duplicate analyses of the samples is generally <3% for the REEs and <5% for the other trace and major elements. We used two U.S. Geological Survey standards to determine the internal and external precision. BCR-1 (basalt rock standard) and SDO-1 (shale standard) were used because the elemental concentrations were known and previous work [*Hannigan and Basu*, 1998] supports the use of the standards in retaining accuracy and maintaining precision in our analyses. We found the published SDO-1 values for the elements under investigation to be within 2–5% of the analyzed results by our ICP-MS methods. Thus, we are confident our analyses have an overall precision and accuracy better than 5%.

4.2. Sr and Nd Isotopes

[13] Samples were accurately weighed into PFA Teflon screw-top beakers (Savillex®) and ^{87}Rb and ^{84}Sr spikes were added quantitatively in order to allow Rb and Sr concentrations to be determined by isotope dilution. Samples were dissolved using HF-HNO_3-HCl. The dissolved sample was accurately aliquoted and the smaller (one third) fraction spiked with ^{145}Nd and ^{149}Sm. Rb and Sr were separated in 2.5 *N* HCl using Bio-Rad AG50W X8 200–400 mesh cation exchange resin. A REE concentrate was collected by elution of 3*N* HNO_3. Nd and Sm were separated in a mixture of acetic acid (CH_3COOH), methanol (CH_3OH) and nitric acid (HNO_3) using Bio-Rad AG1x8 200–400 mesh anion exchange resin. Total procedure blanks for Rb, Sr, Sm and Nd were less than 0.5 ng.

[14] Sr samples were loaded onto single Ta filaments with 1 N phosphoric acid. Rb samples were loaded onto triple Ta filaments. Sm and Nd samples were loaded directly onto triple Ta-Re-Ta filaments. Sr samples were analyzed on a VG Sector 54-30 multiple collector mass spectrometer at the Scottish Universities Environmental Research Centre (SUERC) at East Kilbride. An ^{88}Sr intensity of 1V (1×10^{-11} A) ± 10% was maintained. The $^{87}Sr/^{86}Sr$ ratio was corrected for mass fractionation using $^{86}Sr/^{88}Sr = 0.1194$ and an exponential law. NBS987 gave 0.710255 ± 20 (2σ, n = 21). Rb samples were analyzed on a VG54E single collector mass spectrometer. Three sets of 10 ratios were collected and the mean and standard error computed.

[15] Sm and Nd samples were analyzed on a Micromass IsoProbe multiple collector ICP-MS. $^{143}Nd/^{144}Nd$ ratios were measured with a ^{144}Nd beam of 1V (1×10^{-11} A). Six blocks of 20 ratios were collected in the peak jumping mode and corrected for mass fractionation using an exponential law and $^{146}Nd/^{144}Nd = 0.7219$. Background corrections were applied by measuring on peak zeros in the same 5% nitric acid used to dilute the samples prior to each block of 20 ratios. Repeat analyses of the internal laboratory standard (JM) gave $^{143}Nd/^{144}Nd = 0.511481 \pm 15$ (2σ, n = 21). Nd and Sm concentration (ID) runs were analyzed on a single REE-concentrated solution as three blocks of 20 ratios with ion intensities of >5 ×

Table 1 (Sample). Bulk Sediment Major and Trace Element Chemistry for Modern Sands From the Red River and From a Variety of Cored Paleo-Red River Sedimentary Rocks From the Vicinity of the Red River Delta, Vietnam [The full Table 1 is available in the HTML version of this article at http://www.g-cubed.org]

Sample	Depositional Age, Ma	Lithology	Location	River	SiO_2	TiO_2	Al_2O_3	Fe_2O_3	MnO	MgO	CaO	Na_2O	K_2O	P_2O_5	Total	CIA	V	Cr	Ni
LK 64, 741 m	6.8	siltstone	Hanoi Basin	N/A	74.02	1.07	16.76	7.89	0.13	2.45	1.13	0.49	3.06	0.23	107.23	77.3	67.25	174.38	64.22
LK 81, 1108 m	9.1	sandstone	Hanoi Basin	N/A	93.90	0.60	7.77	3.50	0.08	1.99	2.53	0.34	2.34	0.14	113.18	68.0	42.44	93.63	22.54
LK 41, 444 m	12	sandstone	Hanoi Basin	N/A	93.15	0.82	10.51	4.48	0.08	2.22	3.97	1.44	2.51	0.21	119.37	58.5	68.24	97.18	28.96
LK 108, 1344 m	13.7	siltstone	Hanoi Basin	N/A	78.30	1.03	15.51	6.41	0.14	2.04	1.39	0.62	2.61	0.27	108.32	76.1	82.28	77.61	19.47
LK 200, 2643 m	17	sandstone	Hanoi Basin	N/A	69.79	0.33	4.46	4.92	0.49	2.04	13.81	0.20	1.32	0.53	97.89	68.0	47.58	88.99	24.65
LK 203, 2896 m	24	sandstone	Hanoi Basin	N/A	78.64	0.35	6.01	2.19	0.08	4.25	8.19	0.43	1.61	0.11	101.85	65.5	63.88	79.88	23.31
LK 81, 2250 m	31.5	shale	Hanoi Basin	N/A	55.30	0.98	14.04	5.69	0.13	4.13	11.40	0.16	3.21	0.30	95.35	77.7	127.48	119.9	72.79
LK 206, 2411 m	32	siltstone	Hanoi Basin	N/A	74.51	1.02	16.68	6.18	0.12	2.04	1.72	0.57	3.33	0.23	106.39	75.3	72.14	88.25	27.24
LK 81, 2512 m	33	siltstone	Hanoi Basin	N/A	81.49	0.13	0.74	0.23	0.00	1.09	15.94	0.00	0.34	0.05	100.00	66.8	67.48	143.5	55.99
LK 104, 3590 m	34.8	conglomerate	Hanoi Basin	N/A	88.25	0.78	15.83	5.25	0.05	1.63	0.00	0.06	3.00	0.02	114.88	82.1	26.78	79.03	44.85
LK 106, 3910 m	37	shale	Hanoi Basin	N/A	64.71	0.70	14.49	4.93	0.12	3.76	6.74	0.84	2.49	0.16	98.96	72.6	132.48	58.09	18.15
Pearl					63.92	1.24	19.56	8.38	0.15	1.75	1.08	1.09	2.67	0.21	100.05	75.1	157.45	102.84	97.04
Red River		sand	Hanoi	Red River	80.37	0.65	9.24	3.94	0.05	1.33	1.44	0.83	2.13	0.10	99.98	64.7	65.22	66.05	69.19
VN05060701		sand	Xuan Loc	Song Da	85.48	0.46	6.90	3.18	0.04	0.87	0.60	0.49	1.81	0.08	99.91	65.9	51.81	70.49	51.89
VN05060702		sand	Co Tiet	Red River	80.54	0.64	8.03	3.65	0.07	1.48	2.61	1.02	2.15	0.11	100.30	58.5	60.65	88.95	67.62
VN05060703		clay-silt	Co Tiet	Red River	73.97	0.83	11.29	5.20	0.10	1.88	3.07	1.07	2.42	0.16	99.99	64.7	87.78	104.6	103.31
VN05060704		clay-sand	Minh Quan	Red River	71.27	1.00	12.44	6.31	0.12	1.95	3.04	1.24	2.59	0.19	100.15	64.4	92.24	91.38	141.65
VN05060705		silty sand	N of Yen Bai	Red River	65.27	1.11	15.54	8.41	0.18	2.25	2.88	1.03	2.68	0.21	99.56	71.2	124.43	106.34	63.54
VN05060706		sand	Rail bridge	Small tributary	81.41	0.54	9.04	4.35	0.09	1.39	0.62	0.22	1.96	0.07	99.69	76.0	79.16	70.66	77.02
VN05060707		clay-silt	Ngoi Hut	Small tributary	65.10	1.11	16.57	7.96	0.17	2.21	2.37	0.87	3.03	0.21	99.60	72.9	143.11	130.9	105.97
VN05060708		clay-sand	Ngoi Hut	Red River	63.36	1.23	16.91	9.01	0.18	2.29	2.78	1.03	2.72	0.27	99.78	72.7	132.4	108.2	108.57
VN05060709		sand	Lang Lau	Small tributary	87.49	0.25	6.28	2.12	0.03	0.35	0.25	0.22	3.01	0.03	100.03	61.1	56.71	63.77	79.09
VN05060710		sand	Dan Dhuong	Red River	72.59	0.93	10.75	5.92	0.11	1.83	3.39	1.32	2.45	0.18	99.47	60.6	92.04	72.47	53.15
VN05060801		sand	Lao Cai	Red River	71.93	0.91	12.01	5.98	0.12	1.91	3.37	1.20	2.66	0.17	100.26	63.7	94.01	89.06	69.83
VN05060802		clay with sand	E of Lao Cai	Nam Thip	68.31	0.96	17.87	5.87	0.09	1.21	2.02	0.20	2.93	0.14	99.60	82.3	128.47	129.53	105.73
VN05060803		sand	Gia Phu	Ngoi Bo	75.09	0.67	10.97	5.08	0.07	0.94	1.76	2.08	2.85	0.06	99.57	52.5	74.67	74.12	83.52
VN05060804		fine sand-clay	Pholu Bridge	Red River	65.94	1.06	14.39	7.87	0.16	2.24	3.49	1.34	2.73	0.24	99.46	66.1	92.01	98.88	59.45
VN05060805		sand	Phorang	Song Chay	66.94	0.58	12.76	9.82	0.21	2.07	2.79	0.92	3.44	0.10	99.63	65.4	63.84	71.47	74.08
VN05060806		sand	Bridge	Song Chay	86.29	0.28	6.89	1.65	0.05	0.30	0.42	0.61	2.78	0.05	99.32	57.8	73.45	70.46	64.75
VN05060807		sand	Doan Hung	Song Lo	79.86	0.60	10.00	3.71	0.09	0.87	1.32	0.45	2.71	0.10	99.71	69.3	74.06	85.38	44.83
VN05060808		silty sand	Viet Tri	Red River	72.20	0.82	13.01	5.47	0.11	1.93	2.96	1.11	2.55	0.15	100.31	67.0	96.44	65.05	42.96
VN05060809		sand		Song Lo	84.60	0.41	7.95	2.58	0.05	0.69	0.73	0.67	2.41	0.08	100.17	62.3	46.25	67.56	57.37
VN05061101		sand clay	Ky Son	Song Da	82.20	0.69	8.27	4.19	0.06	1.14	0.94	0.63	1.83	0.10	100.05	67.1	70.12	99.46	73.91

Table 2. Results of Bulk Sediment and Rock Sample Analyses for Nd and Sr Isotopes[a]

Sample	Lithology	Location	River	Latitude, deg	Longitude, deg	$^{143}Nd/^{144}Nd$	% Standard Error	Epsilon Nd	$^{87}Sr/^{86}Sr$	% Standard Error
Pearl River	clay-silt	Guangzhou	Pearl	22.250	113.667	0.512037	0.0016	−11.76	0.723621	0.0014
Red River	sand	Hanoi	Red River	21.850	105.83	0.512044	0.0005	−11.63		
VN05060701	sand	Xuan Loc	Song Da	21.236	105.347	0.512085	0.0009	−10.83	0.720358	0.0016
VN05060702	sand	Co Tiet	Red River	21.285	105.258	0.51212	0.0009	−10.14	0.71664	0.0013
VN05060703	clay-silt	Co Tiet	Red River	21.285	105.258	0.512067	0.0006	−11.18	0.717834	0.0016
VN05060704	clay-sand	Minh Quan	Red River	21.630	104.904	0.512004	0.0018	−12.41	0.715244	0.0011
VN05060705	silty sand	N of Yen Bai	Red River	21.797	104.792	0.512146	0.0005	−9.64	0.717007	0.0013
VN05060706	sand	Rail bridge	small tributary	21.888	104.682	0.511991	0.0007	−12.66	0.730024	0.0013
VN05060707	clay-silt	Ngoi Hut	small tributary	21.968	104.590	0.512125	0.0014	−10.05	0.725472	0.0013
VN05060708	clay-sand	Ngoi Hut	Red River	21.968	104.590	0.512113	0.0008	−10.28	-	-
VN05060709	sand	Lang Lau	small tributary	22.069	104.461	0.511244	0.0025	−27.23	0.713146	0.0012
VN05060710	sand	Tan Thuong	Red River	22.169	104.354	0.511969	0.0009	−13.09	0.715193	0.0013
VN05060801	sand	Lao Cai	Red River	22.503	103.970	0.512089	0.0008	−10.75	0.716533	0.0017
VN05060802	clay/sand	E of Lao Cai	Nam Thi	22.519	103.994	0.511897	0.0009	−14.49	0.737743	0.0013
VN05060803	sand	Gia Phu	Ngoi Bo	22.375	104.077	0.512333	0.0007	−5.99	-	-
VN05060804	sand/clay	Pholu Bridge	small tributary	22.321	104.180	0.512103	0.0006	−10.48	0.713146	0.0012
VN05060805	sand	Phorang	Song Chay	22.235	104.480	0.511951	0.0009	−13.44	0.767424	0.0013
VN05060806	sand	Bridge	Song Chay	21.646	105.186	0.511917	0.0007	−14.10	0.76327	0.0012
VN05060807	sand	Doan Hung	Song Lo	21.622	105.189	0.512061	0.0011	−11.29	0.746864	0.0012
VN05060808	silty sand	Viet Tri	Red River	21.308	105.378	0.512162	0.0006	−9.32	0.717824	0.0012
VN05060809	sand		Song Lo	21.287	105.438	0.511968	0.0008	−13.11	0.749703	0.0019
VN05061101	sand clay	Ky Son	Song Da	20.903	105.351	0.512129	0.001	−9.97	0.71779	0.0014

[a] Nd data for the borehole samples are from *Clift et al.* [2006a].

Table 3. Single Grain K-Feldspar Analyses of Pb Isotopes Made by Ion Microprobe for Grains Taken From Modern River Sands

Sample	River	$^{206}Pb/^{204}Pb$	1 sigma	$^{207}Pb/^{206}Pb$	1 sigma	$^{208}Pb/^{206}Pb$	1 sigma	Pb, ppm	$^{207}Pb/^{204}Pb$	1 sigma	$^{208}Pb/^{204}Pb$	1 sigma	Ba, ppm
VN05061101	Song Da	19.0048	0.102	0.8262	0.003	2.0808	0.012	12.6	15.702	0.102	39.545	0.310	564.4
VN05061101	Song Da	18.4040	0.251	0.8491	0.009	2.1402	0.041	6.9	15.627	0.271	39.388	0.932	7764.1
VN05061101	Song Da	18.6531	0.162	0.8406	0.006	2.0882	0.014	6.4	15.679	0.182	38.952	0.431	10487.3
VN05061101	Song Da	18.4431	0.097	0.8493	0.004	2.1189	0.012	26.6	15.664	0.105	39.080	0.305	630.4
VN05061101	Song Da	18.5416	0.114	0.8402	0.004	2.0898	0.013	11.1	15.578	0.121	38.748	0.333	1960.4
VN05061101	Song Da	18.7780	0.050	0.8336	0.001	2.0891	0.004	58.9	15.654	0.049	39.228	0.130	1692.0
VN05061101	Song Da	18.7780	0.050	0.8336	0.001	2.0891	0.004	58.9	15.654	0.049	39.228	0.130	1692.0
VN05061101	Song Da	18.0747	0.065	0.8685	0.001	2.0922	0.004	53.8	15.698	0.060	37.816	0.152	1857.8
VN05061101	Song Da	18.5281	0.118	0.8449	0.004	2.1023	0.018	42.7	15.654	0.123	38.952	0.411	2011.0
VN05061101	Song Da	18.5875	0.058	0.8386	0.001	2.0920	0.004	42.4	15.587	0.053	38.885	0.141	4858.3
VN05061101	Song Da	18.5242	0.054	0.8461	0.001	2.0977	0.004	42.5	15.673	0.053	38.859	0.132	4166.9
VN05061101	Song Da	18.5843	0.182	0.8251	0.005	2.0551	0.015	5.6	15.334	0.174	38.193	0.472	4792.9
VN05061101	Song Da	18.6734	0.286	0.8393	0.005	2.0912	0.014	1.8	15.673	0.259	39.049	0.649	207.3
VN05061101	Song Da	18.4610	0.036	0.8489	0.001	2.1046	0.003	117.9	15.672	0.037	38.853	0.096	669.4
Hanoi	Song Hong	20.3754	0.160	0.7711	0.005	2.0347	0.016	20.1	15.711	0.161	41.458	0.455	3239.2
Hanoi	Song Hong	18.4563	0.076	0.8481	0.001	2.1042	0.004	34.1	15.654	0.069	38.835	0.173	886.1
Hanoi	Song Hong	18.3226	0.119	0.8522	0.003	2.1251	0.011	29.2	15.614	0.112	38.937	0.319	1355.3
Hanoi	Song Hong	18.5119	0.069	0.8450	0.002	2.0907	0.004	35.8	15.643	0.065	38.703	0.161	1925.4
Hanoi	Song Hong	19.7946	0.158	0.8014	0.004	2.0545	0.021	9.3	15.863	0.151	40.669	0.524	2344.4
Hanoi	Song Hong	18.6909	0.058	0.8344	0.001	2.0735	0.002	43.7	15.596	0.053	38.755	0.127	854.6
Hanoi	Song Hong	18.7675	0.159	0.8239	0.004	2.0644	0.015	4.1	15.462	0.156	38.743	0.431	339.6
Hanoi	Song Hong	18.4401	0.067	0.8490	0.003	2.1160	0.010	708.1	15.656	0.076	39.019	0.238	241.6
Hanoi	Song Hong	18.3591	0.143	0.8486	0.007	2.1164	0.030	66.6	15.580	0.172	38.854	0.623	263.7
Hanoi	Song Hong	18.7318	0.065	0.8367	0.001	2.0893	0.003	33.2	15.674	0.057	39.137	0.145	1608.6
Hanoi	Song Hong	18.5676	0.150	0.8571	0.006	2.1171	0.022	28.7	15.914	0.165	39.310	0.520	7788.5
Hanoi	Song Hong	18.5166	0.112	0.8517	0.005	2.1258	0.021	32.6	15.770	0.133	39.363	0.449	679.5
Hanoi	Song Hong	17.3253	0.187	0.8868	0.005	2.2750	0.024	19.6	15.363	0.191	39.416	0.597	1927.3
Hanoi	Song Hong	17.6658	0.238	0.8617	0.008	2.1177	0.024	9.8	15.222	0.246	37.412	0.661	8140.5
Hanoi	Song Hong	18.9089	0.146	0.8209	0.004	2.0648	0.014	9.6	15.523	0.140	39.043	0.396	918.3
VN05060801	Song Hong	18.5404	0.047	0.8435	0.001	2.1048	0.002	39.2	15.639	0.043	39.023	0.109	6215.8
VN05060801	Song Hong	18.3855	0.039	0.8469	0.001	2.1093	0.003	56.8	15.571	0.037	38.781	0.096	4812.9
VN05060801	Song Hong	18.9883	0.053	0.8205	0.001	2.0510	0.002	44.7	15.580	0.047	38.945	0.117	1725.2
VN05060801	Song Hong	18.8456	0.115	0.8303	0.005	2.1066	0.012	54.2	15.648	0.128	39.701	0.331	3038.6
VN05060801	Song Hong	18.4080	0.110	0.8431	0.004	2.0952	0.014	17.3	15.520	0.114	38.568	0.341	259.0
VN05060801	Song Hong	18.1236	0.057	0.8586	0.001	2.1193	0.003	30.4	15.561	0.052	38.410	0.136	2382.7
VN05060801	Song Hong	18.6003	0.068	0.8377	0.002	2.0780	0.005	35.9	15.581	0.068	38.651	0.170	205.0
VN05060801	Song Hong	18.1310	0.056	0.8576	0.001	2.1106	0.004	39.1	15.549	0.053	38.266	0.141	1653.1
VN05060801	Song Hong	18.1029	0.030	0.8592	0.001	2.1189	0.004	128.3	15.554	0.029	38.358	0.103	199.2
VN05060807	Song Lo	19.4534	0.041	0.8044	0.001	1.9728	0.002	83.7	15.649	0.036	38.378	0.093	96.6
VN05060807	Song Lo	18.5184	0.028	0.8430	0.001	2.0850	0.002	119.1	15.610	0.027	38.610	0.067	1363.1
VN05060807	Song Lo	18.5875	0.157	0.8513	0.002	2.0959	0.007	4.5	15.824	0.140	38.958	0.354	370.2
VN05060807	Song Lo	18.4333	0.061	0.8515	0.001	2.0917	0.003	40.9	15.696	0.057	38.558	0.141	1214.7
VN05060807	Song Lo	18.8382	0.034	0.8336	0.001	2.0465	0.001	97.6	15.703	0.032	38.553	0.075	710.4

Table 3. (continued)

Sample	River	$^{206}Pb/^{204}Pb$	1 sigma	$^{207}Pb/^{206}Pb$	1 sigma	$^{208}Pb/^{206}Pb$	1 sigma	Pb, ppm	$^{207}Pb/^{204}Pb$	1 sigma	$^{208}Pb/^{204}Pb$	1 sigma	Ba, ppm
VN05060807	Song Lo	18.3109	0.031	0.8581	0.001	2.1209	0.002	142.2	15.712	0.030	38.835	0.079	2510.5
VN05060807	Song Lo	18.7479	0.069	0.8381	0.002	2.0951	0.003	17.7	15.713	0.065	39.279	0.159	5061.7
VN05060807	Song Lo	18.1486	0.040	0.8602	0.001	2.1247	0.006	86.4	15.611	0.041	38.560	0.133	1447.6
VN05060807	Song Lo	17.3171	0.047	0.8917	0.002	2.1535	0.010	33.7	15.441	0.055	37.292	0.199	2943.7
VN05060807	Song Lo	18.3853	0.038	0.8544	0.001	2.1072	0.002	97.2	15.708	0.034	38.742	0.086	1759.1
VN05060807	Song Lo	18.5913	0.094	0.8421	0.003	2.0949	0.007	8.3	15.656	0.101	38.946	0.240	878.3
VN05060807	Song Lo	18.7290	0.046	0.8379	0.001	2.0515	0.003	50.5	15.693	0.043	38.423	0.108	222.6
VN05060807	Song Lo	19.4658	0.039	0.8088	0.001	1.9810	0.003	72.7	15.743	0.035	38.561	0.092	85.6
VN05060807	Song Lo	18.5842	0.038	0.8451	0.001	2.0891	0.003	87.8	15.706	0.036	38.825	0.096	1247.0
VN05060807	Song Lo	18.2890	0.044	0.8617	0.001	2.1233	0.004	72.7	15.760	0.043	38.833	0.121	1238.8
VN05060807	Song Lo	18.2116	0.045	0.8622	0.001	2.1227	0.004	65.4	15.701	0.045	38.659	0.117	1485.0
MC-01-75	Yangtze	18.5182	0.079	0.8387	0.003	2.0755	0.012	22.0	15.530	0.087	38.434	0.271	11377.7
MC-01-75	Yangtze	18.4463	0.047	0.8459	0.001	2.0917	0.004	22.9	15.604	0.047	38.584	0.118	5952.1
MC-01-75	Yangtze	18.8502	0.196	0.8289	0.007	2.0805	0.023	4.6	15.626	0.213	39.218	0.599	2072.3
MC-01-75	Yangtze	18.5614	0.150	0.8433	0.003	2.0787	0.009	4.2	15.652	0.140	38.583	0.357	3403.9
MC-01-75	Yangtze	18.9324	0.166	0.8281	0.005	2.0676	0.016	4.4	15.678	0.170	39.145	0.462	566.6
MC-01-75	Yangtze	18.6100	0.055	0.8340	0.002	2.0731	0.007	17.9	15.521	0.057	38.580	0.172	2318.4
MC-01-75	Yangtze	18.4678	0.194	0.8442	0.003	2.0903	0.009	2.8	15.591	0.171	38.603	0.437	790.3
MC-01-75	Yangtze	18.7473	0.061	0.8348	0.002	2.0761	0.008	68.7	15.650	0.063	38.922	0.196	998.3
MC-01-75	Yangtze	18.2486	0.048	0.8475	0.001	2.0893	0.002	50.9	15.465	0.043	38.126	0.105	15248.2
MC-01-75	Yangtze	18.6010	0.173	0.8267	0.007	2.0789	0.022	47.0	15.378	0.189	38.669	0.543	7439.9
MC-01-75	Yangtze	18.4004	0.041	0.8453	0.001	2.0966	0.003	63.4	15.554	0.040	38.578	0.100	1264.8
MC-01-75	Yangtze	18.5454	0.067	0.8351	0.003	2.0665	0.005	35.0	15.488	0.074	38.323	0.167	547.9
MC-01-75	Yangtze	18.5658	0.205	0.8479	0.009	2.1300	0.032	46.3	15.742	0.236	39.545	0.735	1070.5
MC-01-75	Yangtze	18.4626	0.050	0.8475	0.001	2.0904	0.002	51.5	15.648	0.044	38.594	0.110	697.1
MC-01-75	Yangtze	18.2415	0.106	0.8528	0.003	2.1139	0.008	70.1	15.557	0.106	38.561	0.267	3970.0
MC-01-75	Yangtze	18.9471	0.144	0.8210	0.005	2.0430	0.018	48.5	15.556	0.150	38.708	0.447	336.2
MC-01-75	Yangtze	18.4011	0.211	0.8397	0.004	2.0842	0.009	1.7	15.451	0.191	38.352	0.470	201.5
MC-01-75	Yangtze	18.4631	0.092	0.8433	0.003	2.0679	0.012	48.8	15.570	0.092	38.180	0.293	1623.4
MC-01-75	Yangtze	18.4065	0.040	0.8405	0.001	2.0780	0.004	53.0	15.471	0.041	38.250	0.109	1479.1
MC-01-75	Yangtze	18.4976	0.216	0.8532	0.007	2.0947	0.028	42.5	15.782	0.230	38.746	0.687	4161.1
MC-01-75	Yangtze	18.2651	0.044	0.8513	0.001	2.1142	0.004	60.5	15.549	0.043	38.616	0.116	1309.3
MC-01-75	Yangtze	18.4155	0.120	0.8503	0.004	2.1161	0.011	16.7	15.659	0.131	38.968	0.328	964.2
MC-01-75	Yangtze	18.4330	0.040	0.8439	0.002	2.1201	0.005	94.3	15.555	0.044	39.080	0.123	620.3
MC-01-75	Yangtze	18.2034	0.025	0.8557	0.001	2.0915	0.004	119.8	15.576	0.031	38.072	0.083	2402.7
MC-01-75	Yangtze	18.8205	0.162	0.8371	0.005	2.0860	0.023	105.8	15.754	0.160	39.259	0.555	1193.9
MC-01-75	Yangtze	18.2719	0.085	0.8518	0.004	2.1084	0.015	31.9	15.564	0.097	38.524	0.326	2635.3
MC-01-75	Yangtze	18.7728	0.111	0.8407	0.005	2.0750	0.017	21.0	15.782	0.129	38.953	0.396	1907.9
MC-01-75	Yangtze	18.3200	0.451	0.8265	0.015	2.0252	0.058	22.9	15.141	0.461	37.102	1.397	7160.9
MC-01-75	Yangtze	18.5246	0.064	0.8414	0.002	2.0619	0.004	37.6	15.587	0.062	38.195	0.151	1491.2
MC-01-75	Yangtze	18.3825	0.102	0.8456	0.004	2.1032	0.015	30.5	15.544	0.113	38.662	0.354	2383.3

Table 4. Single Grain K-Feldspar Analysis of Pb Isotopes Made by Ion Microprobe for Grains From Sedimentary Rocks From the Hanoi Basin and Northern Gulf of Tonkin

Sample	Stratigraphic Age	$^{206}Pb/^{204}Pb$	1 sigma	$^{207}Pb/^{206}Pb$	1 sigma	$^{208}Pb/^{206}Pb$	1 sigma	Pb, ppm	$^{207}Pb/^{204}Pb$	1 sigma	$^{208}Pb/^{204}Pb$	1 sigma	Ba, ppm
Wushi 21-1-1	Eocene	18.762	0.031	0.840	0.001	2.080	0.004	60.880	15.767	0.036	39.028	0.099	454.9
Wushi 21-1-1	Eocene	18.907	0.076	0.828	0.002	2.051	0.007	24.324	15.651	0.074	38.780	0.202	747.1
Wushi 21-1-1	Eocene	18.972	0.193	0.820	0.006	2.029	0.017	6.912	15.549	0.192	38.499	0.505	65.9
Wushi 21-1-1	Eocene	18.331	0.149	0.854	0.005	2.114	0.016	41.938	15.662	0.160	38.754	0.427	236.1
Wushi 21-1-1	Eocene	17.340	0.046	0.883	0.001	2.158	0.004	59.482	15.312	0.044	37.419	0.124	2028.8
Wushi 21-1-1	Eocene	18.589	0.547	0.804	0.024	2.008	0.069	16.635	14.953	0.630	37.322	1.692	1066.3
Wushi 21-1-1	Eocene	19.853	0.396	0.804	0.015	1.957	0.047	16.858	15.958	0.437	38.849	1.207	806.1
Wushi 21-1-1	Eocene	18.194	0.196	0.846	0.006	2.081	0.010	4.930	15.388	0.200	37.867	0.449	35.3
Wushi 21-1-1	Eocene	18.732	0.083	0.837	0.004	2.082	0.015	29.987	15.685	0.103	39.004	0.330	1889.7
Wushi 21-1-1	Eocene	18.710	0.062	0.839	0.001	2.075	0.003	68.729	15.696	0.055	38.831	0.144	896.5
Wushi 21-1-1	Eocene	18.413	0.125	0.841	0.003	2.073	0.010	28.016	15.491	0.120	38.173	0.323	967.9
Wushi 21-1-1	Eocene	18.341	0.112	0.860	0.005	2.126	0.015	57.995	15.770	0.138	38.992	0.358	1416.9
Wushi 21-1-1	Eocene	18.446	0.214	0.844	0.007	2.101	0.027	18.130	15.577	0.221	38.757	0.671	501.5
Wushi 21-1-1	Eocene	18.629	0.152	0.849	0.006	2.106	0.020	53.409	15.813	0.176	39.242	0.494	1700.9
Wushi 21-1-1	Eocene	18.350	0.046	0.847	0.001	2.076	0.003	69.513	15.536	0.043	38.092	0.114	319.5
Wushi 21-1-1	Eocene	18.516	0.056	0.839	0.001	2.068	0.005	55.150	15.539	0.055	38.287	0.143	1858.0
Wushi 21-1-1	Eocene	17.623	0.050	0.879	0.001	2.098	0.004	97.450	15.494	0.048	36.976	0.127	3331.0
Wushi 21-1-1	Eocene	19.178	0.080	0.821	0.003	2.016	0.010	39.494	15.749	0.083	38.668	0.245	211.5
Wushi 21-1-1	Eocene	19.001	0.173	0.820	0.005	2.028	0.017	29.171	15.588	0.166	38.540	0.476	319.4
Wushi 21-1-1	Eocene	18.452	0.039	0.845	0.001	2.089	0.003	87.213	15.596	0.041	38.538	0.101	1130.6
LK 203, 2896 m	L. Miocene	18.252	0.033	0.859	0.001	2.128	0.005	81.358	15.683	0.037	38.837	0.115	2324.1
LK 203, 2896 m	L. Miocene	18.634	0.185	0.838	0.008	2.095	0.036	37.940	15.624	0.209	39.038	0.776	8410.2
LK 203, 2896 m	L. Miocene	18.274	0.051	0.853	0.001	2.095	0.004	26.288	15.588	0.050	38.276	0.132	1191.0
LK 203, 2896 m	L. Miocene	18.430	0.069	0.854	0.001	2.113	0.004	17.249	15.732	0.065	38.942	0.165	4.2
LK 203, 2896 m	L. Miocene	18.456	0.136	0.847	0.006	2.098	0.022	18.726	15.637	0.157	38.724	0.498	1960.5
LK 203, 2896 m	L. Miocene	21.154	0.119	0.737	0.002	2.143	0.008	12.972	15.595	0.097	45.342	0.312	356.5
LK 200, 2643 m	M. Miocene	18.610	0.051	0.838	0.001	2.088	0.003	45.197	15.594	0.050	38.848	0.125	7461.0
LK 200, 2643 m	M. Miocene	18.461	0.051	0.848	0.001	2.088	0.003	40.934	15.657	0.050	38.542	0.122	1619.6
LK 200, 2643 m	M. Miocene	18.669	0.099	0.832	0.005	2.068	0.022	88.884	15.525	0.118	38.601	0.466	8149.5
LK 200, 2643 m	M. Miocene	19.328	0.088	0.809	0.002	2.063	0.005	11.054	15.642	0.083	39.879	0.210	342.5
LK 200, 2643 m	M. Miocene	18.904	0.146	0.826	0.003	2.096	0.006	8.073	15.606	0.130	39.616	0.328	2348.2
LK 200, 2643 m	M. Miocene	18.778	0.175	0.831	0.004	2.089	0.013	4.329	15.604	0.163	39.235	0.440	8592.5
LK 200, 2643 m	M. Miocene	19.266	0.190	0.809	0.006	2.054	0.024	3.994	15.595	0.196	39.573	0.609	1827.9
LK 81, 1108 m	U. Miocene	18.827	0.057	0.833	0.001	2.077	0.006	55.989	15.681	0.055	39.107	0.162	706.6
LK 81, 1108 m	U. Miocene	18.757	0.058	0.831	0.002	2.075	0.007	78.591	15.594	0.057	38.923	0.172	1371.9
LK 81, 1108 m	U. Miocene	18.418	0.120	0.850	0.003	2.095	0.010	14.636	15.658	0.115	38.586	0.314	530.4
LK 81, 1108 m	U. Miocene	18.321	0.116	0.842	0.005	2.128	0.029	35.583	15.433	0.132	38.990	0.581	3478.9
LK 81, 1108 m	U. Miocene	18.430	0.117	0.839	0.004	2.087	0.012	17.632	15.454	0.121	38.466	0.331	5995.2
LK 81, 1108 m	U. Miocene	19.027	0.050	0.822	0.001	2.075	0.004	57.891	15.633	0.045	39.480	0.129	2153.6
LK 81, 1108 m	U. Miocene	18.301	0.029	0.855	0.001	2.110	0.002	111.55	15.649	0.027	38.622	0.075	1708.1
LK 81, 1108 m	U. Miocene	16.683	0.059	0.913	0.001	2.282	0.003	21.344	15.226	0.058	38.068	0.145	9376.0
LK 81, 1108 m	U. Miocene	18.211	0.077	0.854	0.003	2.098	0.009	14.414	15.557	0.083	38.208	0.237	658.2

Table 4. (continued)

Sample	Stratigraphic Age	$^{206}Pb/^{204}Pb$	1 sigma	$^{207}Pb/^{206}Pb$	1 sigma	$^{208}Pb/^{206}Pb$	1 sigma	Pb, ppm	$^{207}Pb/^{204}Pb$	1 sigma	$^{208}Pb/^{204}Pb$	1 sigma	Ba, ppm
LK 81, 1108 m	U. Miocene	18.658	0.043	0.828	0.001	2.078	0.004	29.928	15.448	0.045	38.780	0.121	4851.2
LK 81, 1108 m	U. Miocene	18.943	0.049	0.826	0.001	2.031	0.003	62.419	15.642	0.045	38.472	0.113	197.5
LK 81, 1108 m	U. Miocene	18.288	0.070	0.854	0.002	2.134	0.005	24.970	15.610	0.067	39.024	0.173	222.9
LK 81, 1108 m	U. Miocene	18.394	0.031	0.848	0.001	2.104	0.002	71.680	15.597	0.030	38.704	0.078	2304.3
LK 81, 1108 m	U. Miocene	19.220	0.057	0.820	0.001	2.095	0.003	28.522	15.762	0.049	40.265	0.129	2091.0
LK 81, 1108 m	U. Miocene	19.438	0.038	0.805	0.001	1.976	0.003	69.655	15.645	0.034	38.411	0.091	224.9
LK 81, 1108 m	U. Miocene	18.772	0.279	0.790	0.017	1.959	0.054	69.630	14.825	0.391	36.773	1.145	54.9
LK 81, 1108 m	U. Miocene	18.272	0.051	0.845	0.001	2.115	0.003	51.255	15.441	0.046	38.650	0.120	9855.1
LK 81, 1108 m	U. Miocene	18.114	0.038	0.859	0.001	2.118	0.002	71.636	15.564	0.035	38.357	0.090	1855.5
LK 81, 1108 m	U. Miocene	18.537	0.101	0.834	0.003	2.075	0.011	25.713	15.455	0.100	38.473	0.298	2963.5
LK 81, 1108 m	U. Miocene	18.482	0.034	0.847	0.001	2.106	0.003	63.001	15.658	0.033	38.916	0.086	142.1
LK 81, 1108 m	U. Miocene	18.476	0.061	0.848	0.001	2.101	0.005	82.557	15.665	0.056	38.810	0.159	618.0
LK 81, 1108 m	U. Miocene	18.185	0.068	0.856	0.002	2.114	0.009	61.832	15.571	0.068	38.438	0.224	314.6
LK 81, 1108 m	U. Miocene	18.703	0.129	0.838	0.003	2.079	0.008	7.414	15.670	0.120	38.884	0.309	5833.9
LK 81, 1108 m	U. Miocene	18.809	0.073	0.828	0.002	2.090	0.005	40.204	15.583	0.069	39.310	0.183	688.5
LK 81, 1108 m	U. Miocene	18.527	0.033	0.844	0.001	2.089	0.002	106.65	15.641	0.032	38.696	0.080	2887.6
LK 41, 441 m	U. Miocene	18.385	0.060	0.846	0.001	2.079	0.006	30.269	15.559	0.058	38.224	0.168	226.5
LK 41, 441 m	U. Miocene	18.289	0.064	0.849	0.002	2.109	0.008	62.508	15.533	0.065	38.572	0.206	2074.4
LK 41, 441 m	U. Miocene	18.392	0.035	0.850	0.001	2.106	0.003	108.50	15.627	0.036	38.730	0.094	3156.6
LK 41, 441 m	U. Miocene	18.717	0.037	0.831	0.001	2.049	0.003	80.505	15.553	0.038	38.350	0.089	554.8
LK 41, 441 m	U. Miocene	18.327	0.051	0.842	0.001	2.104	0.003	98.423	15.438	0.046	38.568	0.124	5301.8
LK 41, 441 m	U. Miocene	18.185	0.031	0.858	0.001	2.111	0.002	135.83	15.612	0.030	38.389	0.073	44.0
LK 41, 441 m	U. Miocene	18.420	0.045	0.844	0.001	2.080	0.002	82.497	15.541	0.041	38.318	0.102	908.5
LK 41, 441 m	U. Miocene	18.757	0.270	0.793	0.008	2.040	0.021	1.913	14.877	0.266	38.267	0.677	5895.3
LK 41, 441 m	U. Miocene	18.813	0.039	0.823	0.001	2.077	0.002	68.649	15.475	0.038	39.072	0.093	586.0
LK 41, 441 m	U. Miocene	18.837	0.043	0.825	0.001	2.071	0.004	62.129	15.532	0.041	39.014	0.119	4176.2
LK 41, 441 m	U. Miocene	18.577	0.097	0.839	0.005	2.096	0.020	24.201	15.583	0.128	38.930	0.422	3640.5
LK 41, 441 m	U. Miocene	17.577	0.057	0.880	0.001	2.112	0.004	46.805	15.462	0.055	37.128	0.137	4050.3
LK 41, 441 m	U. Miocene	18.217	0.234	0.864	0.013	2.181	0.057	26.479	15.736	0.306	39.736	1.163	1377.5
LK 41, 441 m	U. Miocene	18.015	0.032	0.861	0.001	2.116	0.003	87.056	15.503	0.034	38.112	0.084	962.7
LK 41, 441 m	U. Miocene	18.893	0.071	0.829	0.003	2.071	0.007	72.152	15.668	0.085	39.125	0.195	1349.9
LK 41, 441 m	U. Miocene	19.559	0.213	0.793	0.004	2.064	0.010	3.064	15.509	0.189	40.360	0.481	2926.9
LK 41, 441 m	U. Miocene	17.582	0.170	0.882	0.005	2.270	0.016	5.144	15.509	0.176	39.902	0.479	2685.7
LK 41, 441 m	U. Miocene	18.133	0.075	0.851	0.002	2.122	0.006	10.726	15.439	0.071	38.484	0.193	1096.0
LK 41, 441 m	U. Miocene	16.762	0.041	0.911	0.001	2.150	0.004	60.987	15.269	0.043	36.037	0.112	10299.2
LK 41, 441 m	U. Miocene	18.533	0.039	0.842	0.001	2.084	0.003	61.020	15.605	0.037	38.631	0.099	423.9
LK 41, 441 m	U. Miocene	18.665	0.033	0.833	0.001	2.078	0.002	103.23	15.544	0.031	38.784	0.083	3048.7
LK 41, 441 m	U. Miocene	18.576	0.065	0.831	0.001	2.100	0.004	22.424	15.435	0.060	39.016	0.159	4957.8
LK 41, 441 m	U. Miocene	18.474	0.056	0.832	0.001	2.076	0.003	23.435	15.364	0.050	38.360	0.128	6142.4
LK 41, 441 m	U. Miocene	18.108	0.027	0.857	0.001	2.115	0.003	64.453	15.524	0.029	38.296	0.078	285.8
LK 41, 441 m	U. Miocene	18.500	0.066	0.834	0.001	2.086	0.004	18.920	15.421	0.061	38.590	0.158	6475.3
LK 41, 441 m	U. Miocene	18.730	0.065	0.829	0.002	2.067	0.005	42.426	15.533	0.064	38.708	0.165	2486.7
LK 41, 441 m	U. Miocene	18.654	0.063	0.826	0.001	2.071	0.002	52.086	15.412	0.055	38.640	0.138	1896.7

Table 5. Pb Isotope Analyses of Bulk Sediments From the Hanoi Basin, Measured by ICP-MS

Sample	$^{206}Pb/^{204}Pb$	$^{207}Pb/^{204}Pb$	$^{208}Pb/^{204}Pb$
LK 41, 444 m	18.89466	15.70745	39.46809
LK 81, 1108 m	18.83811	15.72161	39.28490
LK 200, 2643 m	18.79203	15.71457	39.21047

10^{-13}A for ^{143}Nd and ^{149}Sm, respectively. External precision on $^{145}Nd/^{143}Nd$ and $^{149}Sm/^{147}Sm$ is better than 0.01% (2σ, n = 11) based on analyses of a mixed Nd and Sm solution used as an internal standard. Rb, Sr, Nd and Sm isotope ratios are adjusted for mass fractionation/bias and spike contribution. Results of the analysis are shown in Table 2. For data analysis we calculate the parameter ε_{Nd} [*DePaolo and Wasserburg*, 1976] using a $^{143}Nd/^{144}Nd$ value of 0.512638 for the Chondritic Uniform Reservoir [*Hamilton et al.*, 1983].

4.3 Pb Isotopes of Detrital Feldspars

[16] In order to understand better the provenance evolution of the Red River we employ the technique of measuring Pb in situ [*Layne and Shimizu*, 1998] in single K-feldspar sand grains using a high-resolution Cameca 1270 ion microprobe at the University of Edinburgh. Although producing analytical uncertainties much greater than the conventional thermal ionization mass spectrometer (TIMS) method, the ion microprobe approach allows isotopic determinations on individual sand and silt-sized particles, which are below the size possible with TIMS. In order to exploit the potential of this method to characterize heterogeneous feldspar populations several analyses were run from each sample in order to define the range of isotopic ratios in a single sample, and to identify small populations of grains with distinct isotopic characters (Table 3).

[17] Sand and disaggregated sandstones were sieved, after which the 1 mm to 100 μm size fractions was mounted in epoxy and polished using aluminum oxide abrasives. The K-feldspar grains were then identified by area mapping of Al_2O_3 and K_2O using the JEOL *Superprobe* electron microprobe at the Massachusetts Institute of Technology. This allowed the K-feldspars to be identified for isotopic analysis. After gold coating the grains were analyzed using a beam of negatively charged oxygen ions (O^-) focused to a spot as small as 15–20 μm. The analyses were calibrated using analyses of glass from standards SRM610 and DR4-2. In addition, 22 repeat measurements were made on a Shap granite feldspar previously characterized by *Tyrrell et al.* [2006]. Analytical uncertainties are principally a reflection of the counting statistics, typically averaging $2\sigma \leq 1\%$. The analytical results are shown in Tables 3 and 4.

[18] In order to minimize the risk of secondary Pb contamination from sources outside the feldspar, analyses were made in the center of each grain, away from cracks, inclusions or alteration zones. Because we only analyze unaltered material sediment eroded from strongly weathered sources will be underrepresented. Feldspar is susceptible to chemical weathering and breakdown compared to more stable minerals, such as quartz or zircon, so that our method introduces a bias that favors sources experiencing rapid physical weathering. The ion beam was trained on the spot to be analyzed for five minutes before analysis began, so that any surface Pb contamination that might have occurred during preparation of the grains mount was removed. Through probing grain centers and allowing the beam to remove surface coating of the sectioned grains we avoid analysis of excess secondary Pb that is normally removed by leaching procedures prior to conventional mass spectrometry [*Gariepy et al.*, 1985].

4.4. Bulk Sediment Pb Isotopes

[19] Three samples were selected for bulk sediment analysis of Pb isotopes. Approximately 0.3 g of powdered sample were dissolved in a mixture of 3:1 HF and HNO_3, dried down with concentrated HNO_3, 6.2N HCl and concentrated HBr before being transferred to vials for column separation. Pb was separated by anion exchange using the HNO_3-HBr procedure of *Galer* [1986] and *Abouchami et al.* [1999]. Pb analyses were performed on the NEPTUNE multicollector ICP-MS at Woods Hole Oceanographic Institution (WHOI) using thallium to correct for instrumental mass discrimination. Pb analyses carry internal precisions on $^{206}Pb/^{204}Pb$, $^{207}Pb/^{204}Pb$ and $^{208}Pb/^{204}Pb$ ratios of 15–30 ppm; and external reproducibility (including full chemistry) ranges from 17 ppm (2σ) for $^{207}Pb/^{206}Pb$, to 117 ppm (2σ) for $^{208}Pb/^{204}Pb$. Pb ratios were adjusted to the SRM981 values of *Todt et al.* [1996]. Results from this work are shown in Table 5.

5. Results

5.1. Weathering Proxies

[20] The strength of chemical weathering in the Red River basin can be assessed by consideration

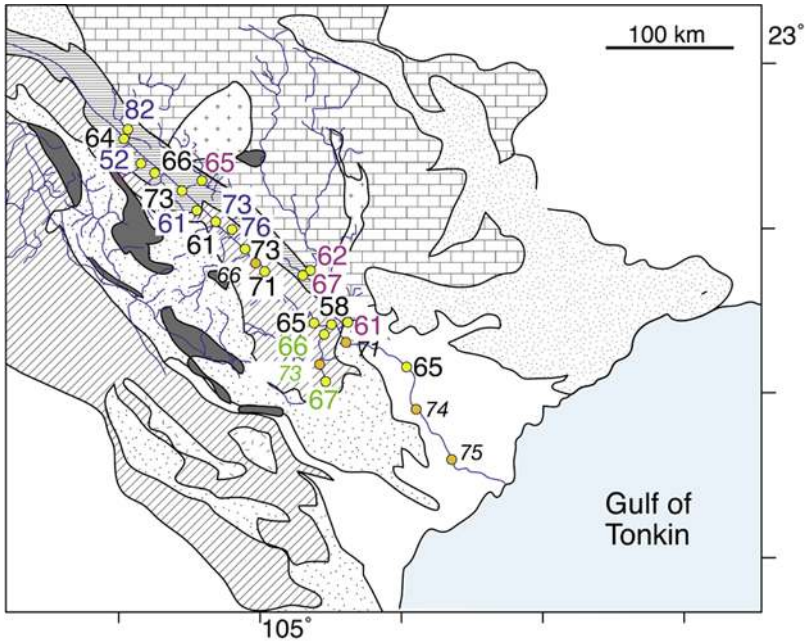

Figure 5. Geological map of the Red River basin overlain by an outline of the major river courses (blue line) and showing variations in chemical weathering intensity. See Figure 3 for legend to the geological units. Numbers show the calculated Chemical Index of Alteration (CIA) of *Nesbitt and Young* [1982]. Yellow dots show samples taken during this study, while orange dots and smaller, italic script show samples analyzed by *Liu et al.* [2007]. These latter samples are all fine-grained lithologies. Samples from the trunk Red River are denoted by black numbers, while small tributaries are shown in blue. Samples from the Song Da and Song Lo are shown as green and pink text, respectively.

of the Chemical Index of Alteration (CIA) a proxy developed by *Nesbitt and Young* [1982], which is based on the relative mobility of Na, K and Ca in aqueous fluids, compared to immobile Al, which tends to be concentrated in the residues of weathered rocks. CIA is calculated as follows:

$$\mathrm{CIA} = \frac{\mathrm{Al_2O_3}}{(\mathrm{Al_2O_3} + \mathrm{CaO^*} + \mathrm{Na_2O} + \mathrm{K_2O})} \times 100$$

[21] CIA is derived from the molecular weights of the oxides. The CaO* value used is only the calcium content from the silicate fraction of the sediment and correction must be made for the carbonate and phosphate contents. No attempt was made to dissolve carbonate before analysis. In this study we follow the method of *Singh et al.* [2005] in using P_2O_5 to correct for phosphate. Subsequently, a correction is made for carbonate based on assuming a reasonable Ca/Na ratio for silicate continental material. If the remaining number of moles after the phosphate correction is still more than the number of Na_2O moles then this latter value is used as a proxy for CaO* value. Uncertainties in the CIA values are in excess of the 3% uncertainty in the XRF analytical data and can be used only as general proxies for weathering intensity.

[22] Figure 5 shows a map of the Red River basin with the calculated values of CIA marked at their sampling location. Colors are used to distinguish between the trunk river and the different tributaries that contribute to this stream. CIA is quite low in the upper reaches (Figure 2) with a value of 64 being shown near Lao Cai, suggesting that physical weathering is dominating the erosion in the upper reaches. However, some of the smaller tributaries show much higher values of CIA, up to 82, suggesting that chemical weathering is intense along the middle reaches of the river, at least at lower elevations. Low CIA values are also seen in some of the larger tributaries, such as those draining the Day Nui Con Voi (Figure 2), indicative of strong physical weathering in the higher ranges.

[23] CIA values recorded by *Liu et al.* [2007] are mostly higher than those found in this study, but this is mostly a grain size effect, reflecting the focus of that study on muds, while this study is directed more at sands and silts. CIA barely changes downstream from 64 at Lao Cai (Figure 5) to 65 in sands near Hanoi, although higher values are seen

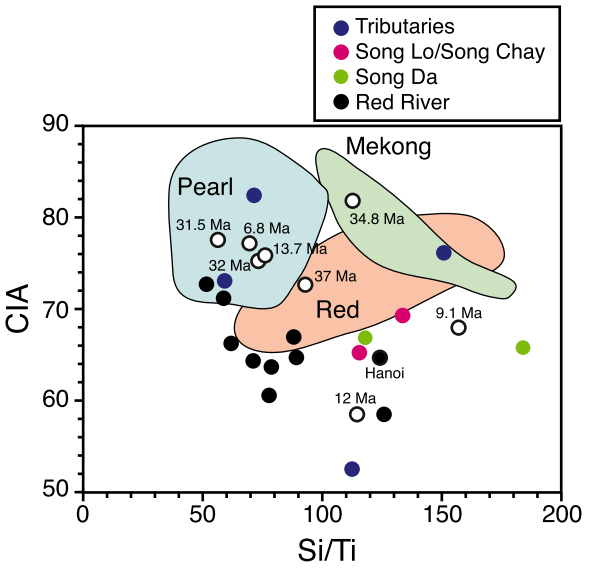

Figure 6. Discrimination plot showing Chemical Index of Alteration (CIA) plotted against Si/Ti for all samples considered in this study. Fields for modern trunk Red, Mekong, and Pearl rivers are from *Liu et al.* [2007] and include only fine-grained sediments. Black circles show values from borehole rocks in the Hanoi Basin, labeled with depositional age. Note modern river sample from Hanoi, which is the most downstream sample considered here.

locally in the river between these points. Higher CIA values associated with stronger chemical weathering are seen in small tributaries and in the Song Da (66), neither of which appear to dominate the flux in the trunk river. The variability in CIA in each drainage system makes their influence on the bulk flow to the ocean impossible to quantify accurately.

[24] Plotting Si/Ti (a ratio independent of the carbonate content) versus CIA allows the different parts of the Red River drainage to be compared with one another (Figure 6). *Liu et al.* [2007] demonstrated that CIA was lower in the Red compared to the Pearl and Mekong rivers, reflecting a more physically erosive environment. Our data generally plot at similar Si/Ti ratios but lower CIA values than *Liu et al.*'s [2007] data. A general negative trend in Si/Ti versus CIA within the sediments from the main Red River suggests a mineralogical control on CIA. Sandier, quartz-rich sediments tend to have lower CIA values, while *Liu et al.*'s [2007] clays have higher CIA. The highest CIA values seen are found in the smaller tributaries, equivalent to values seen in the Mekong and Pearl rivers. The borehole samples show a wide range of CIA values, although the older samples generally show higher CIA. The modest number of samples and lithological variability makes definition of coherent temporal trend impossible (Table 1).

[25] Sr isotope character can also be used to trace chemical weathering intensity because this at least partially reflects the weathering intensity in silicates, as well as the proportion of carbonate to silicate in the source regions, i.e., the provenance [*Derry and France-Lanord*, 1996]. In Figure 7 we plot the evolving downstream variations in $^{87}Sr/^{86}Sr$ ratio, showing how the composition of the trunk stream changes as more tributaries join this. What is striking is that the Red River is remarkably stable in $^{87}Sr/^{86}Sr$ values until its confluence with the Song Lo, which together with the Song Chay shows much higher $^{87}Sr/^{86}Sr$ values than other parts of the basin. Although the $^{87}Sr/^{86}Sr$ of the Red River falls again after its peak just below that confluence, the Sr budget of the river is permanently disrupted by the flux from the Song Lo.

5.2. Interpretation of Weathering Data

[26] Our data support the suggestion by *Liu et al.* [2007] that the Red River is less influenced by chemical weathering than the neighboring Pearl and Mekong rivers. However, by extending the analysis further upstream than before we can see that much of that signal is inherited from erosion in the upper reaches of the catchment, i.e., upstream of Lao Cai (Figure 2). High CIA values in some lowland tributaries demonstrate that strong chemical weathering is occurring at lower elevation, but that rivers bringing such material to the mainstream comprise a small proportion of the total clastic load reaching the ocean. Chemical weathering appears to have been quite variable in the past, with generally higher intensities seen prior to 30 Ma and at 6.8 and 13.7 Ma, although lithological variability makes this conclusion weakly supported.

[27] Interpretation of the Sr isotope data is complicated because this isotope system is controlled by both weathering intensity and provenance. The high $^{87}Sr/^{86}Sr$ values of Song Lo and Song Chay sediments may indicate stronger chemical weathering in this part of the drainage compared to the Song Da and upper Red River. However, it should be remembered that the Song Lo drains large regions of Paleozoic carbonates on the edge of the relatively ancient Yangtze Craton and that provenance could account for much of the ob-

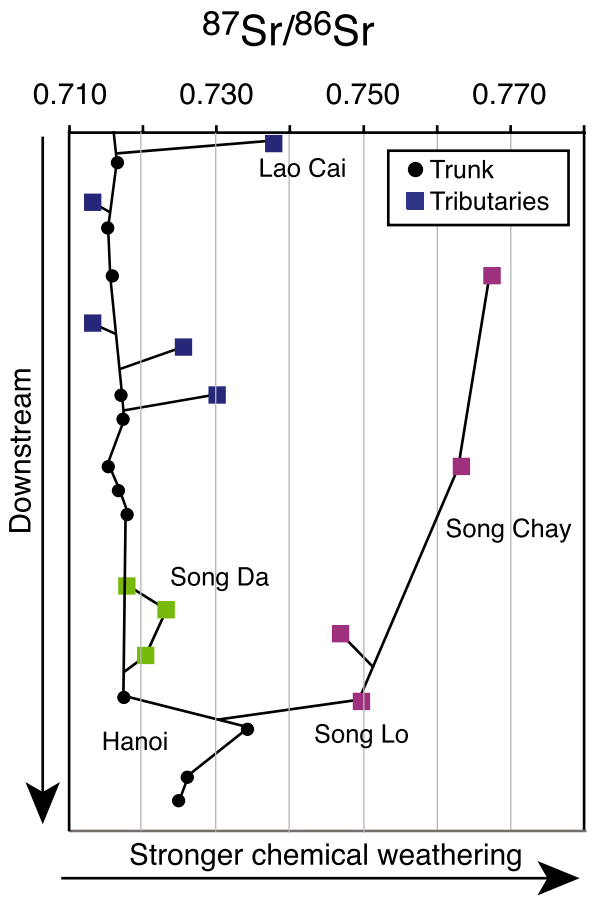

Figure 7. Chart showing downstream variation in Sr isotope composition of the Red River. Samples from the trunk river are marked as black dots, while small tributary samples are displayed as blue squares. Those from the Song Lo and Song Da are shown in pink and green, respectively.

served isotopic differences. A simple mixing calculation indicates that around 50% of the Sr immediately downstream of the Song Lo-Red River confluence is from the Song Lo. Even further downstream the proportion contributed from the Song Lo is estimated at ~25%. In contrast, the Song Da is not important to the Sr budget because its isotopic value lies close to that of the Red River trunk stream. As a result, even before damming the Song Da is not expected to have been important in changing bulk $^{87}Sr/^{86}Sr$ values reaching the South China Sea, but may well have been important to other aspects of the net Red River flux.

[28] The relationship between $^{87}Sr/^{86}Sr$, weathering intensity and provenance can be assessed by comparing $^{87}Sr/^{86}Sr$ values with CIA (Figure 8a). This plot shows no systematic relationship between Sr isotopes and chemical weathering. In contrast, Figure 8b shows a clear link between Sr concentrations and $^{87}Sr/^{86}Sr$ values, with low $^{87}Sr/^{86}Sr$ values only found in high Sr concentration sediments. This relationship indicates a provenance control on $^{87}Sr/^{86}Sr$. This hypothesis can be further tested using Nd isotopes because Nd is mostly water-immobile and thus immune to weathering process. This isotope system is a well-accepted provenance proxy. Figure 8c shows that there is a loosely defined trend to lower ε_{Nd} values with higher $^{87}Sr/^{86}Sr$ values, supporting the idea that provenance is the principle control over Sr. However, the trend shows significant scatter. One sample from the main Red River just south of Lao Cai shows an ε_{Nd} value of −13 and a $^{87}Sr/^{86}Sr$ value of 0.715193. At the same time we note a sample from the Song Chay where ε_{Nd} is only slightly higher, at −13.4, but where $^{87}Sr/^{86}Sr$ is much higher at 0.767424.

6. Provenance Proxies

6.1. Rare Earth Elements

[29] Rare earth element (REE) data from the sediments are best displayed using a multielement diagram normalized against a C1 chondrite standard. In Figure 9 we show the modern river sediment normalized against the values of *Anders and Grevesse* [1989]. Our analyses show a largely coherent and limited range of REE characteristics. Light rare earth element (LREE) enrichment is ubiquitous, as might be expected for a river eroding a wide area of upper continental crust. There is a common slight Eu depletion and many of the samples are quite similar to one another. A relative enrichment in Gd, Tb and Dy is visible, especially in the sample taken at Hanoi, but is also seen to a less degree in the Song Da and in some of the smaller tributaries (Samples VN05060709 and VN05060804). These samples show a clear slope in the medium and heavy rare earth elements (HREEs). The Song Lo in contrast shows a rather flat pattern in the HREEs, but with a steep relative enrichment in the LREEs.

[30] The REE character of the borehole samples is shown in Figure 10. For reference we also plot the modern river sand sample from Hanoi. Nearly all the paleo-river sediments show modest LREE enrichment, with the exception of the youngest 6.8 Ma sample (LK 64, 741 m). Relative Eu depletion is less well displayed compared to the modern sediments and is only prominent in Sample LK 200, 2643 m. This pattern is likely the product

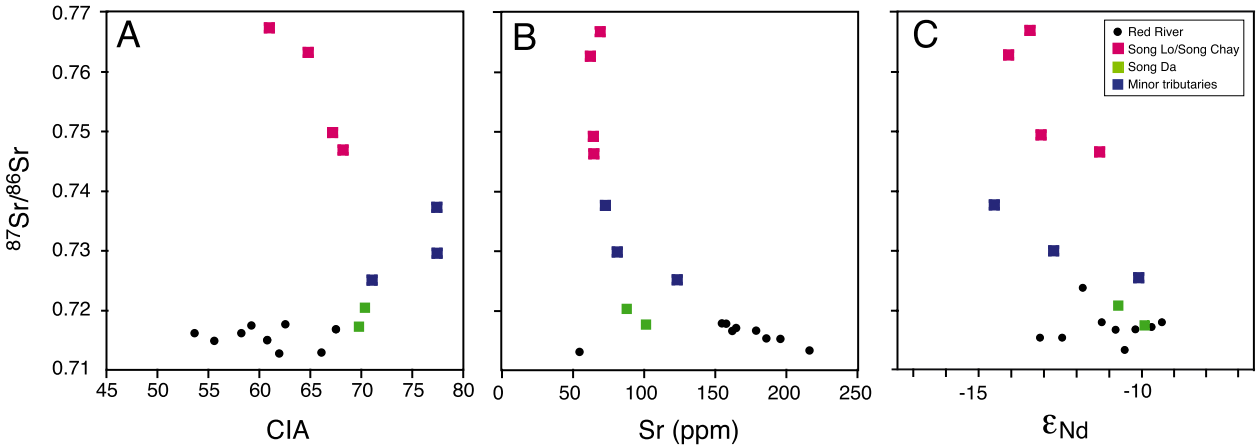

Figure 8. Plots of $^{87}Sr/^{86}Sr$ (a) versus CIA, (b) versus Sr concentrations, and (c) versus ε_{Nd} for modern Red River sediments. Plots demonstrate a poorly defined trend to lower ε_{Nd} with higher values of $^{87}Sr/^{86}Sr$, and a strong linkage between Sr contents and $^{87}Sr/^{86}Sr$.

of mineral sorting removing feldspars from the sand.

[31] In order to compare modern and ancient samples we have plotted a proxy of LREE enrichment (La/Yb) against TiO_2 contents (Figure 11a). TiO_2 is concentrated in oxide minerals and is a reflection of their contribution to the bulk mineralogy. La/Yb indicates the general degree of LREE enrichment of the whole sediment. Figure 11a shows that the Song Da sediments are somewhat more LREE-enriched than most other sediments in the modern river, but lie close to those from the

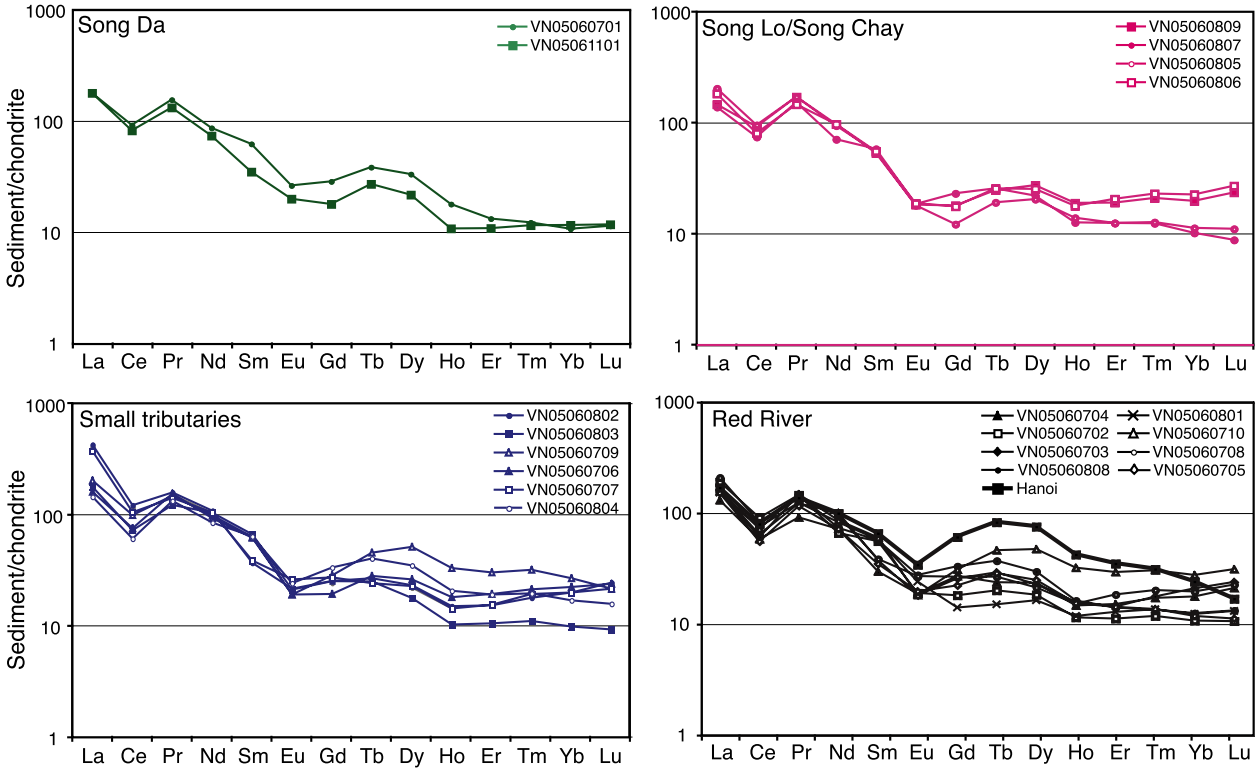

Figure 9. Chondrite normalized rare earth element figure for sediment taken from the modern Red River. Sediments are divided into groups: those from the southern Song Da system, those from the northern Song Lo and Song Chay system, those from smaller tributaries, and those from the main trunk river. Chondrite values used are from *Anders and Grevesse* [1989]. Data are shown in Table 1.

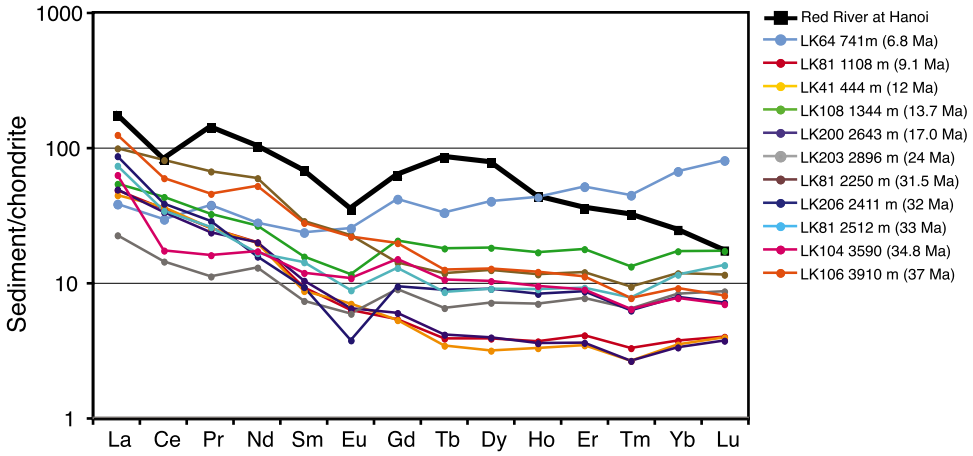

Figure 10. Chondrite normalized rare earth element figure showing the range of compositions in Hanoi Basin of sedimentary rocks. Legend shows depositional age. Chondrite values used are from *Anders and Grevesse* [1989]. Data are shown in Table 1.

borehole dated at 37, 12 and 9.1 Ma. The trunk Red River shows a spread of La/Yb values, but has generally higher TiO_2 contents compared to the tributaries. The Hanoi sample shows one of the lowest La/Yb ratios, though close to those from the Song Lo. The very low TiO_2 contents seen in the borehole samples dated at 17, 24 and 33 Ma reflect lithology, as these are generally sandier and more quartz rich. There is no coherent temporal evolution visible in the borehole samples. In practice the REE compositions of the river sediments do not appear to be effective provenance proxies because there is little coherency in the variations.

6.2. Nd Isotopes

[32] Nd isotopes have a long history of application to sedimentary provenance studies because this element is typically not considered as being mobile in aqueous fluids. In addition, weathering and the sediment transport processes are not expected to result in isotopic fractionation. As a result the measured isotopic signature of any given sediment should reflect the bulk composition of the source and is not altered by reaction with water [*Goldstein et al.*, 1984]. The successful application of Nd isotopes to constraining the provenance of fluvial marine sediments eroded from other parts of Neogene Asia [*Clift et al.*, 2006a; *Colin et al.*, 1999; *Li et al.*, 2003] suggests that this method is appropriate for constraining sediment sources in the Red River. Here we synthesize our results with those of *Liu et al.* [2007] in order to generate a more complete image of Nd isotope variation in the Red River.

[33] Figure 12 shows the range of values in ε_{Nd} for all sediments in the Red River basin. There is significant variability in ε_{Nd} values along the course of the river, yet the ε_{Nd} value of −11.5 seen closest to the delta is only slightly higher than the −10.8 found in the trunk stream at Lao Cai. However, there is significant isotopic variability in

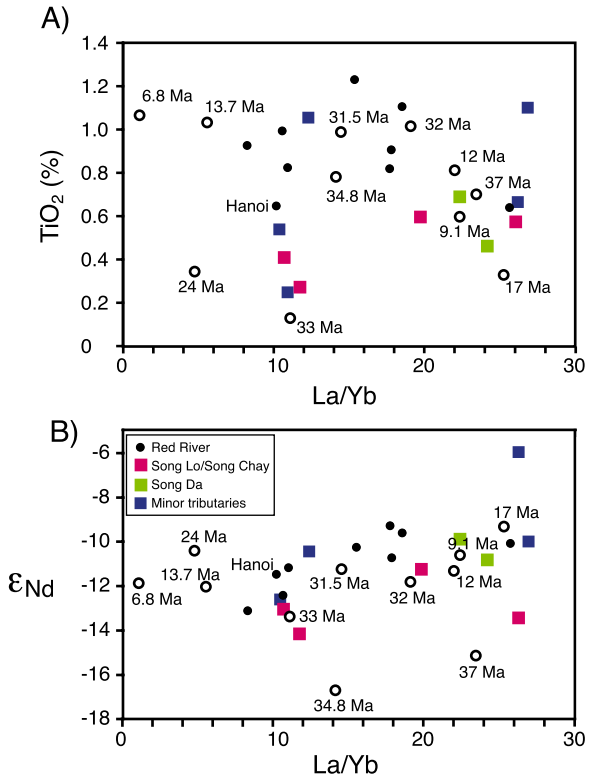

Figure 11. (a) Plot of TiO_2 versus La/Yb and (b) plot of La/Yb versus ε_{Nd} for modern and ancient Red River sediments.

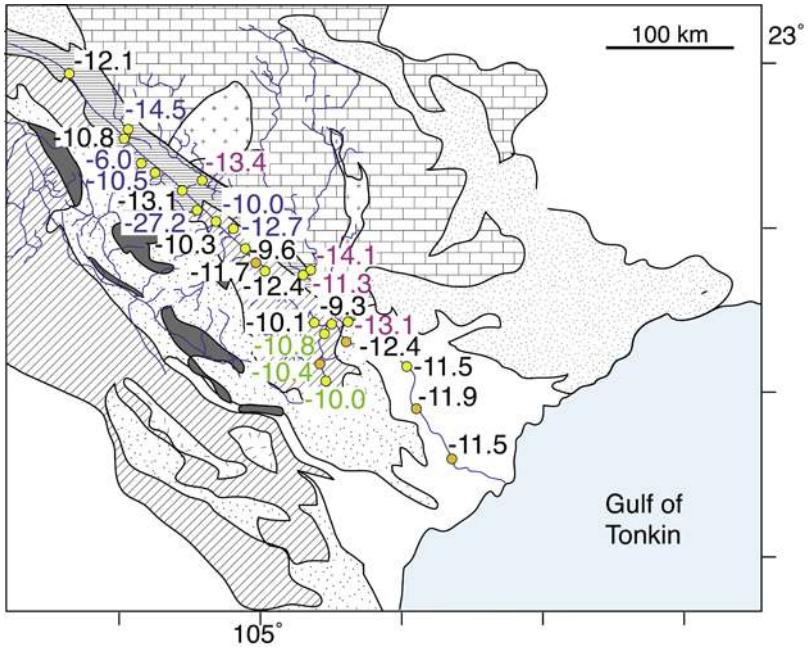

Figure 12. Map showing variability in Nd isotopes along the course of the Red River. See Figure 3 for legend to the geological units. Yellow dots show samples taken during this study, while orange dots denote samples analyzed by *Liu et al.* [2007]. Samples from the trunk Red River are marked by black numbers, while small tributaries are shown in blue. Samples from the Song Da and Song Lo are shown as green and pink text, respectively. Data are shown in Table 2.

the sources and the smaller tributaries. As a rule more negative values (−14.5 to −11.3 and indicative of erosion from older, radiogenic continental crust), are seen in the northern Song Lo and Song Chay, while higher ε_{Nd} values (−10.8 to −10.0, associated with more primitive crust), are seen in the Song Da. As might be expected the most extreme values are found in the smaller tributaries, ranging from an ε_{Nd} value of −27 to as high as −6. These values indicate small-scale crustal heterogeneity, which is averaged out in the larger catchments. One particularly high ε_{Nd} value of −6 suggests the presence of primitive crust; perhaps ophiolites or primitive, mantle-derived lavas, within that catchment. Conversely very low values (ε_{Nd} = −27) are equivalent to ancient cratonic crust, such as found in the Yangtze Craton [*Chen and Jahn*, 1998; *Ma et al.*, 2000], and is lower than is typical of basement known from the Indochina Block [*Lan et al.*, 2003].

[34] Direct comparison of sediment ε_{Nd} values with bedrock values is difficult because of the wide variability known from outcrop (Figure 13a). Statistical methods can be used to assess the range of possibilities and to determine a "typical" fingerprint for each source. It can be seen that many rocks in SE Asia have ε_{Nd} values between −18 and −4 but that most sources have significant spread within that range. This makes Nd a less powerful provenance tool in SE Asia than in some areas where there is wider separation between different sources. Nonetheless, downstream variations can be used to constrain sediment budgets. Figure 13b shows that the main Red River evolves from an ε_{Nd} value of about −11 near Lao Cai to −11.5 near the delta. Curiously the shifts in ε_{Nd} value during the passage rarely seem to reflect the composition measured in the small tributaries, indicating inputs from sources that we have not measured. The overall stability of the ε_{Nd} values indicate that the small tributaries do not affect the total budget greatly. As might be expected the composition of the river downstream of the Song Lo confluence is an important exception and demonstrates that this is an important contributor to the net sediment flux.

6.3. Pb Isotopes

[35] In order to better understand the provenance of the modern Red River we measured Pb isotopes in situ in single sand grains of K-feldspar using a high-resolution ion microprobe. K-feldspar was chosen because it is a common detrital mineral and contains relative high concentrations of Pb that

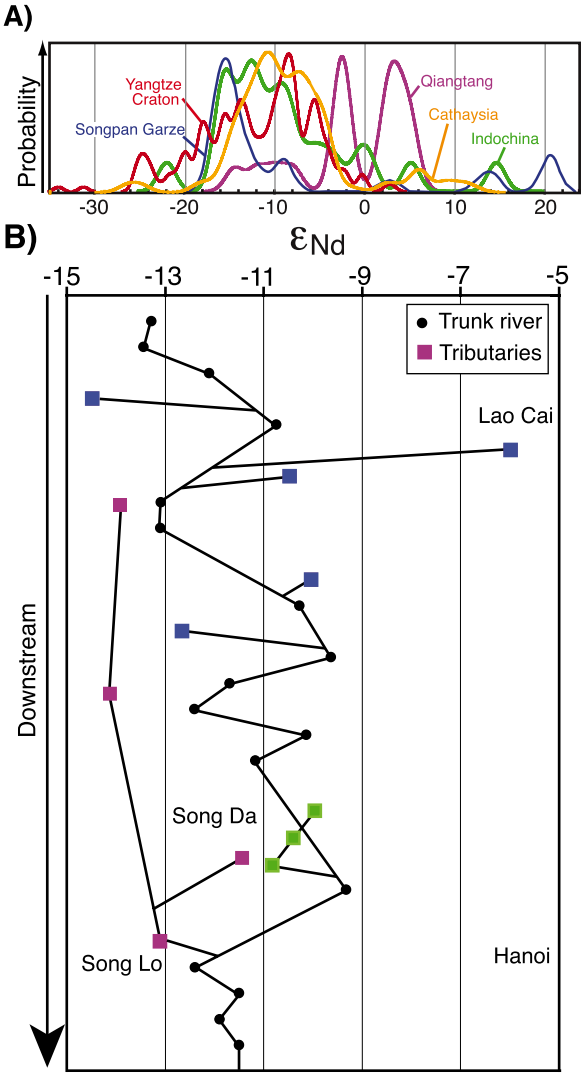

Figure 13. (a) Nd isotopic compositional ranges of possible source terrains in the paleo-Red River. Yangtze Block data are from *Ma et al.* [2000] and *Chen and Jahn* [1998]. Indochina data are from *Lan et al.* [2003]. Cathaysia data are from *Chen and Jahn* [1998], *Darbyshire and Sewell* [1997], *Li et al.* [2002], and *Gilder et al.* [1996]. Qiangtang Block data are from *Roger et al.* [2003], *Li et al.* [2004], and *Bai et al.* [2005]. Songpan Garze block data are from *Huang et al.* [2003b]. (b) Chart showing downstream variation in Nd isotope composition of the Red River. Samples from the trunk river are marked as black dots, while small tributary samples are displayed as blue squares. Those from the Song Lo and Song Da are shown in pink and green, respectively.

allow accurate isotopic determination. Its use as a provenance indicator has been proven through earlier studies using both conventional thermal ionization mass spectrometer (TIMS) [*Hemming et al.*, 1998; *McDaniel et al.*, 1994] and ion probe [*Clift et al.*, 2002]. In order to exploit the potential of this method to characterize heterogeneous feldspar populations several analyses were run from each sample in order to define the range of isotopic ratios and to identify small populations of grains with distinct isotopic characters. Statistically >50 grains should be analyzed from a mixed sediment to accurately image the diversity at the 95% confidence limit [*Ruhl and Hodges*, 2005]. Unfortunately we do not have this number of grains here, yet the influence from different end-member sources is still resolvable and even a limited array can be combined with other data to suggest likely provenance solutions, especially with regard to the dominant, if not the minor grain populations.

[36] Figure 14 shows the results from analysis of five modern river sands, four being parts of the Red River system and one from the upper Yangtze. In each case the detrital grain compositions are compared with known isotopic fields for basement rocks in SE Asia, although such data are rather sparse. The locations of the blocks are shown in Figure 1, except for the Transhimalaya, which lie along the southern edge of Tibet, adjacent to the course of the modern Yarlung Tsangpo, and the Konga Shan, which is a granite massif, located in the SE corner of the Songpan Garze terrane. We also show the mantle arrays for the Indian and Pacific Oceans for reference, and compare with sand samples from the Red River near Hanoi, as well as from the upper reaches of the Mekong and Salween rivers measured by conventional TIMS [*Bodet and Schärer*, 2001].

[37] Our results show a range, which overlaps with that of *Bodet and Schärer* [2001], but with some outliers not detected in the earlier study. Our analysis of the Red River in Hanoi shows a significant number of grains plotting with lower $^{207}Pb/^{204}Pb$ ratios compared to those found by *Bodet and Schärer* [2001] (Figure 14d). More striking is the analysis of the Red River at Lao Cai, where a number of high-quality analyses show little overlap with the *Bodet and Schärer* [2001] field, but a reasonable match to several of our analyses from the Hanoi area (Figure 14c). In contrast, the Song Lo shows a dominant grouping of higher $^{207}Pb/^{204}Pb$ ratios, distinct from the Lao Cai group, and with great overlap with the analyses of *Bodet and Schärer* [2001] (Figure 14b). The Song Lo grains have similar isotope characteristics to those measured from the Lhasa Block, the Konga Shan and the Songpan Garze terrane of eastern Tibet [*Roger*, 1994; *Roger et al.*, 1995]. Although this river does not erode these regions its

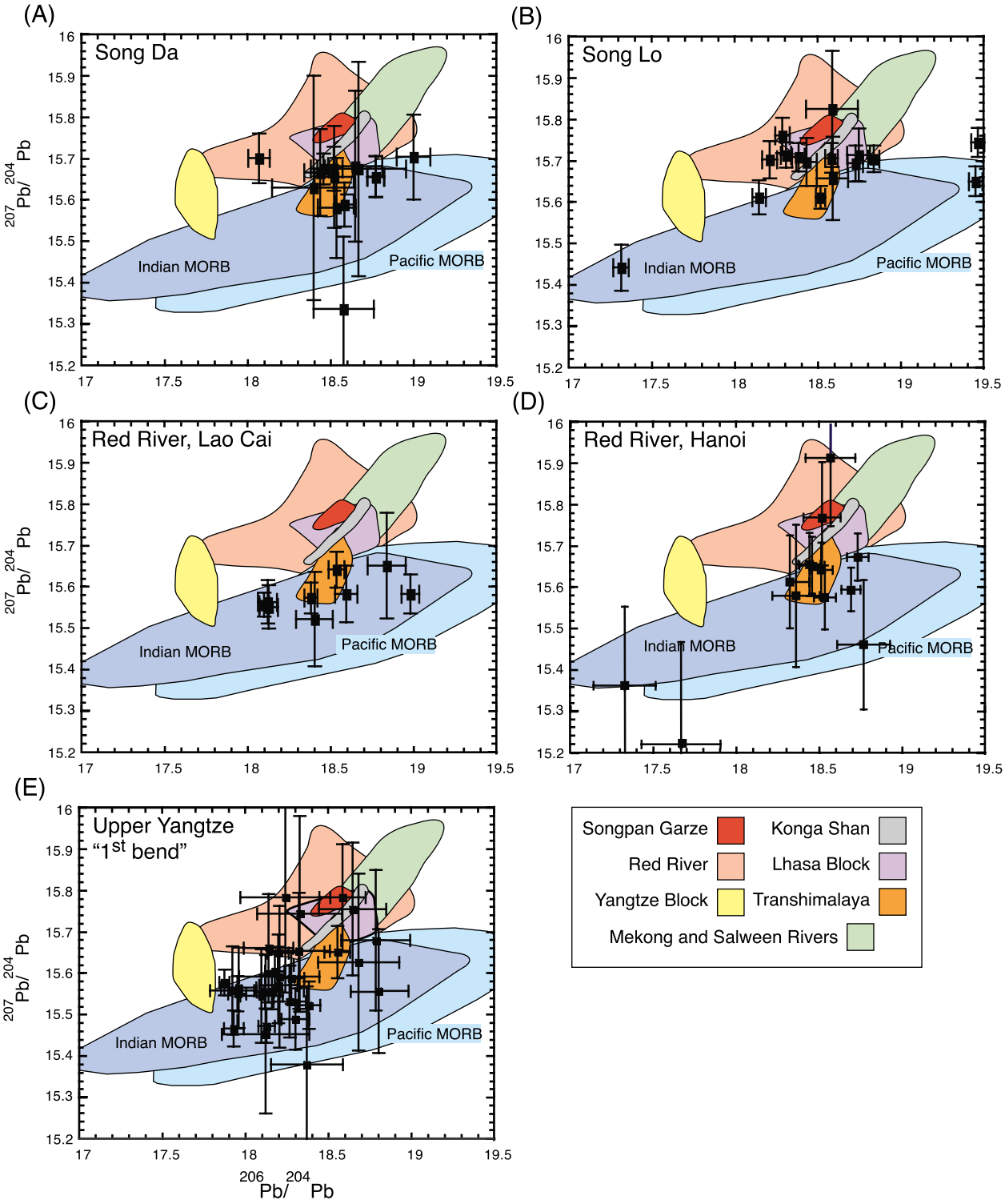

Figure 14. Pb isotope discrimination diagram showing the range of compositions measured from single K-feldspar grains in the Red River, its major tributaries, and the Yangtze River at its first major bend. See Figures 2 and 3 and Table 2 for the locations of the samples. Uncertainties shown are 1 sigma. Field for modern Red River is defined from *Bodet and Schärer* [2001]. Analyses from Songpan-Garze Flysch Belt and the Yangtze Block are from *Roger* [1994]; those from the Transhimalaya are from *Vidal et al.* [1982] and *Gariepy et al.* [1985], while those from the Konga Shan are from *Roger et al.* [1995]. MORB fields are from *Sun* [1980], *Ben Othman et al.* [1989], *Mahoney et al.* [1992], and *Castillo et al.* [1998].

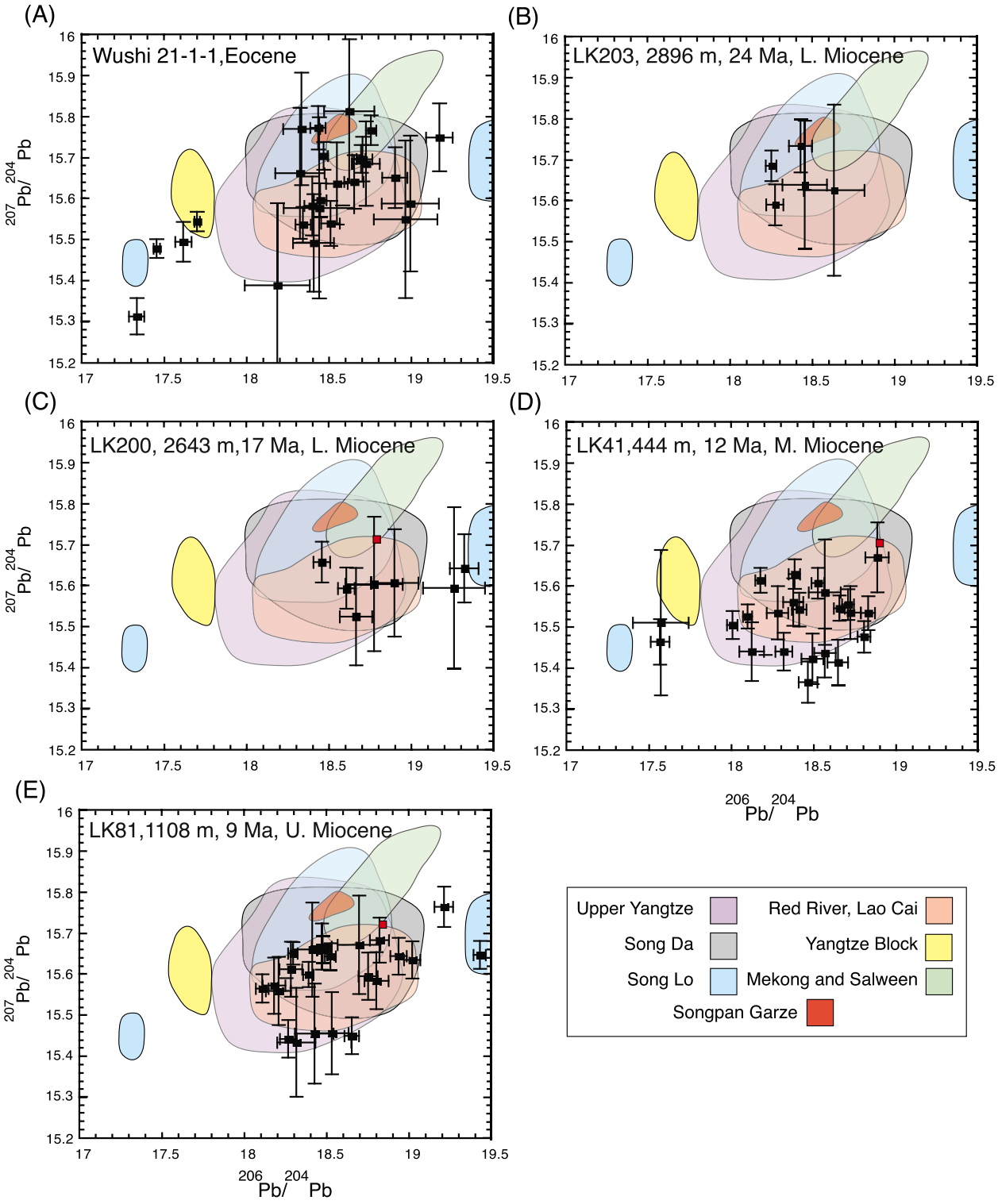

Figure 15. Pb isotope discrimination diagram showing the range of compositions measured from single K-feldspar grains extracted from sandstones at a number of stratigraphic levels within the Hanoi Basin. Colored fields show the range of values measured from the tributaries of the Red River and upper Yangtze River, shown in Figure 14. Fields for the Mekong and Salween rivers are from *Bodet and Schärer* [2001]. Red squares show Pb composition of bulk sediment samples.

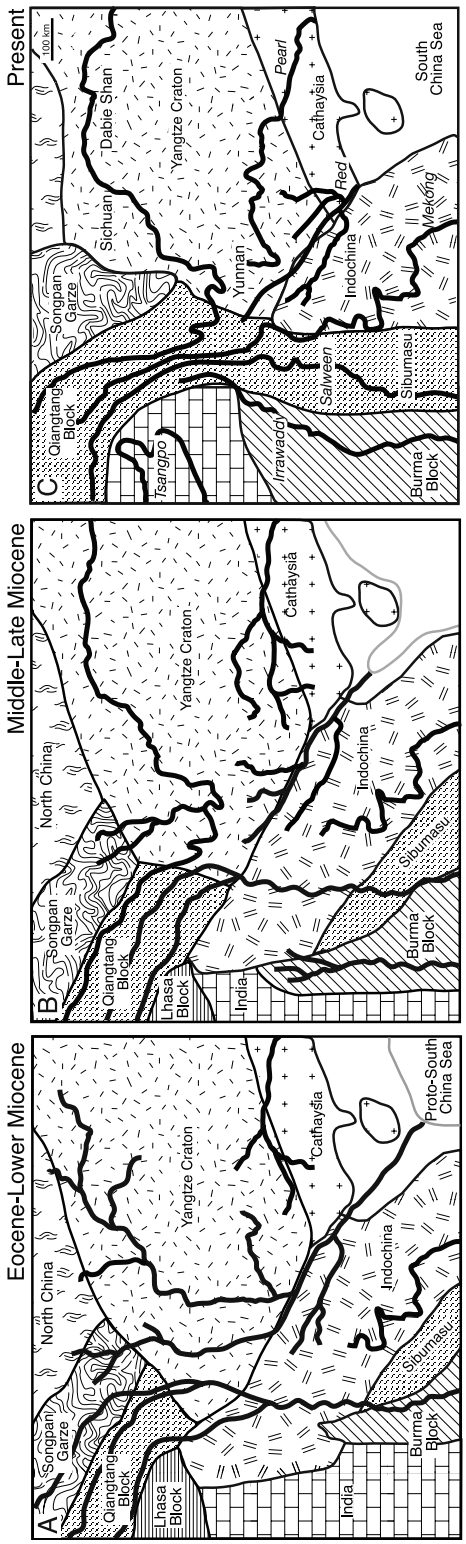

Figure 16. A series of paleogeographic maps showing a possible series of drainage patterns that would be compatible with the geochemical data presented here, modified after the model of *Clark et al.* [2004]. (a) Eocene-Lower Miocene, (b) Middle and Upper Miocene, (c) present-day. Reconstruction of major tectonic blocks taken from *Hall* [2002] and *Replumaz and Tapponnier* [2003].

sources are isotopically identical and may be along-strike equivalents.

[38] The isotopic range identified from the upper Yangtze (Figure 14e) shows overlap with the Red River grains, but with a dominant population displaced to lower $^{207}Pb/^{204}Pb$ and $^{206}Pb/^{204}Pb$ ratios, potentially making its influence in a paleo-Red River resolvable from the other source regions.

[39] Analyses of sand grains from a subset of the borehole samples are shown in Figure 15. In addition to the single grain analyses we show bulk sediment Pb isotope analyses for samples LK 200, LK 41 and LK 81. Surprisingly these latter analyses all plot in a similar place on the all isotope diagrams. Bulk sample analyses do not appear to be closely related to the change distribution of the K-feldspar grains and have limited provenance use. In Figure 15 we compare the sands with the fields defined by the major modern rivers, as well as with the upper Mekong and Salween [*Bodet and Schärer*, 2001] and basement measurements from the Yangtze Craton [*Roger*, 1994], as being potentially representative of areas that were once part of the paleo-Red River, but which have now been lost. Two samples, dated as Eocene and Middle Miocene (Figures 15a and 15d) contain grains with low $^{206}Pb/^{204}Pb$ ratios (<17.8) that are not common in the modern rivers. This may suggest drainage loss of such sources from the modern system. However, we note that one well defined grain of this composition was found in the modern Song Lo (Figure 14b) and two less accurately constrained grains of this age were found in the modern Red River sand from Hanoi (Figure 14d). As a result drainage evolution is not required to explain their presence in the Eocene and Middle Miocene samples.

[40] Very few grains fall within the range of values seen in the upper Salween and Mekong (which are indistinguishable from one another), with the possible exception of the Eocene sand (Figure 15a). The youngest two sands LK 41, 444 m (Middle Miocene) and LK 81, 1108 m (Upper Miocene) show a relatively close correspondence to the modern Red River at Lao Cai, but do not show grains with higher $^{207}Pb/^{204}Pb$ ratios, such as seen in the Song Lo and lower reaches of the Red River.

7. Provenance Synthesis

7.1. Patterns of Modern Erosion

[41] Although they do not identify end-members the Nd bulk sediment data still provide important

controls on where the sediment in the modern Red River is being eroded. In this respect they are more useful than the more random REE data. The drop in ε_{Nd} values in the Red River downstream of the Song Lo confluence shows that this tributary is a major supplier of sediment to the trunk stream. A simple mixing calculation using samples up and downstream of the confluence would indicate that ~80% of the Nd budget comes from the Song Lo. However, the Red River stabilizes at slightly higher ε_{Nd} values downstream. If the ε_{Nd} value of −11.5 is taken as more representative of the lower Red River then this implies that ~40% of the modern clastic load is derived from the Song Lo. It should be noted that because our study focuses on the bed load sediments the budget for the suspended sediments could potentially be quite different.

[42] The influence of the Song Da is harder to assess because of the Hoa Binh dam and because the ε_{Nd} value of the Red River downstream of the Song Da confluence is even less negative than the highest sediment ε_{Nd} value seen in the Song Da meaning that its value cannot be explained by simple mixing of the sediments measured upstream of the confluence. Nonetheless, the strong shift to higher ε_{Nd} values in the Red River downstream of the Song Da confluence does suggest that this is an important contributor of material and must have been more so prior to damming. In contrast, the smaller tributaries between Hanoi and Lao Cai, eroding the Day Nui Con Voi, do not appear to disturb the Nd budget to a measurable degree. Similarly they make no perceptible impression on the Sr budget. Such a result is in accord with the suggestion by *Clift et al.* [2006b] that the upper reaches of the Red River in China are the most important sources of sediment to the delta. Monsoon precipitation is heavy in the Day Nui Con Voi, yet this alone is insufficient to drive rapid erosion. Instead active rock uplift is required as well. Rapid neotectonic deformation is noted in the upper reaches of the Red River in Yunnan and northern Vietnam, associated with the Red River and Song Chay Faults [*Chen et al.*, 1999; *Wang and Ye*, 2006]. In addition, there is recent uplift of the Song Chay metamorphic dome linked with reversal of motion on the Red River Fault Zone [*Replumaz et al.*, 2001] and which may be responsible for the faster erosion seen in the Song Chay-Song Lo system [*Maluski et al.*, 2001].

7.2. Evolving Drainage Patterns

[43] The Pb isotope data from the boreholes are strongly indicative of drainage capture affecting the Red River since the Eocene. Our new data confirm the suggestion by *Clift et al.* [2004] that the Eocene contains a minority population of grains with low $^{206}Pb/^{204}Pb$ ratios, which are most consistent with erosion from the Yangtze Craton. This would require reverse flow from the middle Yangtze into the Red River [*Clark et al.*, 2004]. However, our work shows that such grains can also be found in the modern Song Lo, though still presumably eroded from the Yangtze Craton. It is the association with low ε_{Nd} values in the Eocene and the mismatch in eroded and sedimented volumes [*Clift et al.*, 2006a] that makes the case for major drainage reorganization and suggests the middle Yangtze as the source of these grains, rather than the Song Lo. Two low $^{206}Pb/^{204}Pb$ grains are also found in the 12 Ma Middle Miocene sample (Figure 13d), but are not seen in the 9 Ma Upper Miocene sample. There are insufficient grains analyzed from the 24 and 17 Ma samples to be sure that this grain population is not present at those times. The disappearance of low $^{206}Pb/^{204}Pb$ grains suggests additional drainage capture between 12 and 9 Ma. Assuming the middle Yangtze was lost prior to the Early Miocene [*Clift et al.*, 2006a] then the reorganization between 12 and 9 Ma must involve another tributary draining from the NE into the Red River. It is noteworthy that neither of the 12 or 9 Ma sands contains grains with high $^{207}Pb/^{204}Pb$ ratios, as typify the modern Song Lo. This suggests that the Song Lo has only been captured into the Red River after 9 Ma (Figure 16).

[44] Very few grains from the Hanoi Basin that predate Sample LK 41, 444 m (deposited at 12 Ma) plot with Pb isotope compositions typical of the upper Yangtze. Although too few grains were analyzed from Samples LK 200, 2643 m and LK 203, 2896 m (dated at 24 and 17 Ma) for them to be good representatives of the clastic flux the Eocene sample Wushi 22-3-1 yielded 22 analyses, which suggests that there was no connection to those areas now eroded by the upper Yangtze River at that time. Because of the degree of isotopic overlap between the different possible sources we cannot exclude the influence of the upper Yangzte to the Red River before 12 Ma. However, there are regions of isotope space, especially around $^{207}Pb/^{204}Pb$ values of 15.5 and $^{207}Pb/^{204}Pb$ of 18.0, that are uniquely and quite commonly found

in the modern upper Yangtze. Because we do not find grains with that composition in the pre-12 Ma samples there is no compelling case for linking the upper Yangzte to the paleo-Red River at that time. Nonetheless, the isotopic overlap prevents us from excluding the possibility of a connection. We can only conclude that it is not the most likely paleo-drainage pattern.

[45] This preferred model is at odds with that proposed *Clark et al.* [2004], which predicted both the middle and upper Yangtze as having drained into the Red River at this time. Few Eocene grains even plot in the defined range of the upper Salween and Mekong [*Bodet and Schärer*, 2001]. If the upper Yangtze did not connect with the Red River then presumably it must have found an alternative route to the ocean via SE Asia. In turn this prevents a connection between the Yarlung, Salween or Mekong with the paleo-Red River, since they could not cross the Yangtze. Within the constraints of our data there is no compelling evidence of erosion from eastern Tibet in these Eocene sandstones, although a connection with the middle Yangtze seems clearer. The data do allow a connection between the Red River and the Upper Yangtze during the Middle and Upper Miocene (Figure 15d), but this is not required because rocks of this composition are known from the modern upper Red River.

[46] Our new Nd and Pb data can help interpret the Cenozoic Nd evolution seen in the Hanoi Basin [*Clift et al.*, 2006a]. A rise in ε_{Nd} values from −17 to −12 between 37 Ma and 24 Ma was interpreted as reflecting loss of the middle Yangtze from the paleo-Red River. Our data show that none of the major rivers in the modern Red River is capable of supplying ε_{Nd} of −17. This requires significant flux from a region of low ε_{Nd}, such as the Yangtze Craton, to account for the average composition. The rather positive ε_{Nd} values seen in the Qiangtang and Cathaysia Blocks means that erosional flux from these regions cannot have been high in the Oligocene. However, average ε_{Nd} values of around −15 for the Songpan Garze terrane allows this source to have been important as a sediment source to the Red River during the Eo-Oligocene. Pb isotope data broadly support this paleo-drainage pattern (Figure 16), as Eocene grains with high $^{207}Pb/^{204}Pb$ values (Figure 15a) fall within the known Songpan Garze range [*Huang et al.*, 2003a], but are gone before 12 Ma and maybe much earlier. There is little Pb evidence of sediment flux from the Songpan Garze after the Early Miocene.

[47] Our probe data from the Hanoi Basin section indicate at least four phases of erosion. (1) Eocene, (2) Middle Miocene (12 Ma), with no $^{207}Pb/^{204}Pb$ ratios > 15.7, but including grains with $^{206}Pb/^{204}Pb$ ratios < 17.7, (3) Upper Miocene (9 Ma) when the low $^{206}Pb/^{204}Pb$ grains have disappeared, and (4) modern river in which grains with $^{207}Pb/^{204}Pb$ > 15.7 are seen in both TIMS and SIMS analyses. In the modern river the high $^{207}Pb/^{204}Pb$ grains are provided by the Song Lo, which must be captured after 9 Ma into the Red River (Figure 16). The paleo-Song Lo presumably formed an independent river flowing to the South China Sea, or was part of the Pearl River.

[48] The combined isotope data indicate that drainage capture has continued through the Cenozoic. Although *Clift et al.* [2006a] emphasized major capture prior to 24 Ma we show that sediment composition continued to change after that time, even since 9 Ma. This is consistent with the continued mismatch between eroded and deposited volumes of sediment that require the paleo-Red River basin to have been much larger in the past [*Clift et al.*, 2006a]. Although initial topographic uplift of the paleo-Red River basin must have initiated in the Oligocene, as eastern Asia reversed its regional tilt from westward to eastward [*Wang*, 2004], the uplift continues to the present day. There is a general trend of surface uplift becoming younger to the southeast. While gorge cutting in Sichuan has been used to date major uplift there starting at 13–9 Ma [*Clark et al.*, 2005], uplift in the region of the modern Red River is Pliocene and younger [*Schoenbohm et al.*, 2006]. Thus continued drainage capture is a logical outcome of the continuously changing topography in SE Asia during the Cenozoic.

8. Crustal Heterogeneity

[49] Our data provide additional constraints on the nature of crustal heterogeneity in SE Asia. Nd isotopes show a wide variation at small scales but similar averages over wider regions. ε_{Nd} values of the Mekong and Red River deltas are −10.1 and −11.5 [*Clift et al.*, 2006a], while the Pearl and Yangtze yield values of −10.4 and −12.3, respectively [*Liu et al.*, 2007; *Yang et al.*, 2007]. If only the upper Yangtze is considered then the ε_{Nd} value

is around −10.5 [*Clift et al.*, 2004; *Yang et al.*, 2007]. This is a very tight range compared to rivers in south Asia and suggests that with the important exception of the Yangtze Craton much of eastern Asia has similar Nd isotope characteristics. Although the different blocks are separated from one another by Cenozoic and Mesozoic suture zones the Nd isotopes indicate similar timing and processes of crustal generation.

[50] The Nd analysis of Red River tributaries reveals crustal heterogeneity on a variety of scales. Small-scale crustal blocks are revealed within the Day Nui Con Voi, close to the Red River Fault Zone and site of an earlier Triassic suture zone [*Metcalfe*, 1996]. The presence of very low ε_{Nd} values (down to −27) SW of the Red River Fault Zone suggests the presence of fragments of ancient crust, likely Yangtze Craton, in that region. The Song Lo and Song Chay show contrasting Nd, Sr and Pb isotope characteristics compared to the main Red River, especially in its upper reaches, and with the Song Da to the SW. This pattern demonstrates the geochemical separation of Indochina from China and the differences between the Yangtze Craton and most of Tibet. K-feldspar grains from the Song Lo have similar Pb isotope characteristics to those measured from the Lhasa Block, the Konga Shan and the Songpan Garze terrane of eastern Tibet [*Roger*, 1994; *Roger et al.*, 1995]. This may reflect their similar origins as Gondwana crustal blocks accreted to Asia and forming an active margin prior to India-Asia collision.

[51] The Songpan Garze moderately differs in isotope character from the surrounding blocks, reflecting its mixed erosional origin as an accretionary complex sandwiched between north China and the Yangtze Craton [*Weislogel et al.*, 2006; *Zhou and Graham*, 1996]. It is also noteworthy that the Pb isotope characteristics of K-feldspar grains from the upper Yangtze are quite different from those measured in the upper Mekong and Salween River. While *Bodet and Schärer* [2001] demonstrated an isotopic overlap of these latter rivers, the upper Yangtze has lower $^{207}Pb/^{204}Pb$ and $^{206}Pb/^{204}Pb$ ratios compared to those drainages. We conclude that the northern Qiangtang Block has a unique petrological and tectonic history compared to the central and southern regions drained by the Mekong and Salween. Field studies have shown that the north comprises accreted oceanic arc units (e.g., Yidun arc [*Reid et al.*, 2005]) and accretionary complexes [*Kapp et al.*, 2000; *Li and Zheng*, 1993].

9. Conclusions

[52] The data presented here reveal a more detailed understanding of erosion processes in the Red River basin than previously possible. REE data do not appear to be effective provenance poxies. CIA values show no coherent evolution downstream from Lao Cai to Hanoi. This and other proxies for weathering shows that little sediment is added to the trunk river from small streams draining the Day Nui Con Voi in the middle reaches. Chemical weathering measured by CIA appears to be stronger in the Song Da and Song Lo basins. The Song Lo and Song Chay have an especially dramatic effect on the Sr budget of the river. This partially reflects stronger chemical weathering, but is largely a provenance effect, linked to the abundance of Paleozoic carbonates in that region. We calculate that 25% of the Sr reaching the ocean is derived from the Song Lo.

[53] The new Nd and Pb data support the suggestion that most of the erosion in the modern Red River occurs in its upper reaches [*Clift et al.*, 2006b; *Liu et al.*, 2007]. However, our work now highlights the importance of the Song Lo, which supplies 40% of the Nd budget to the delta. Pb isotopes too show how the composition of the trunk river changes downstream of the Song Lo confluence, most notably a shift to higher $^{207}Pb/^{204}Pb$ ratios. The strongest erosion is not located where monsoon rains are heaviest, but only where these are also associated with active rock uplift.

[54] Analysis of Pb isotopes in sedimentary rocks from the Hanoi Basin demonstrates that drainage capture affected the Red River basin during the Neogene, as well as in the Oligocene, as earlier demonstrated by Nd isotopes [*Clift et al.*, 2006a]. Bulk sample Pb analyses do not appear to be closely related to the range found in K-feldspar grains and thus have limited provenance use. Grains with low $^{207}Pb/^{204}Pb$ and $^{206}Pb/^{204}Pb$ ratios are indicative of erosion from the Yangtze Craton and links between the middle Yangtze and Red River during the Eocene and possibly as late as 12 Ma. There is no geochemical evidence to support a connection with the upper Yangtze or with the upper Mekong and Salween, but a link with erosion of the Songpan Garze is consistent

with both Pb and Nd data. Pb compositions typical of grains in the modern Song Lo are not seen until after 9 Ma. Capture of the Song Lo into the Red River may have postdated 6.8 Ma. Prior to this time the Song Lo must have been independent or drained into the Pearl River.

[55] We conclude that combined trace element and isotopic studies can be effective at constraining erosion patterns in modern river systems, but that single isotope systems alone are less powerful. In east Asia Nd is less useful than in south Asia because so many of the sources have similar isotope characters, with the exception of the Yangtze Craton and Cathaysia block.

Acknowledgments

[56] We thank the Natural Environment Research Council (NERC) for supplying analytical time on the Edinburgh ion probe facility. We thank Anne Kelly and Vincent Gallagher for their help in the Sr and Nd analysis. National Science Foundation (NSF) provided travel funding for Clift to visit Vietnam and collect samples. Clift thanks the Alexander Von Humboldt Foundation for their support of his time at the University of Bremen to complete the writing of this paper. The paper was improved thanks to comments by Christophe Colin and two anonymous reviewers.

References

Abbey, S. (1983), Studies in "Standard Samples" of silicate rocks minerals 1969–1982, *Geol. Surv. Can. Pap.83-15*, 1–114, Ottawa.

Abouchami, W., S. J. G. Galer, and A. Koschinsky (1999), Pb and Nd isotopes in NE Atlantic Fe-Mn crusts: Proxies for trace metal paleosources and paleocean circulation, *Geochim. Cosmochim. Acta*, *63*, 1489–1505, doi:10.1016/S0016-7037(99)00068-X.

Anders, E., and N. Grevesse (1989), Abundances of the elements: Meteoric and solar, *Geochim. Cosmochim. Acta*, *53*, 197–214, doi:10.1016/0016-7037(89)90286-X.

Bai, Y., L. I. Li, Z. Niu, and J. Cui (2005), Characteristics and tectonic setting of Eerlongba Formation volcanic rocks in Geladandong area of Central Qiangtang, *Acta Geosci. Sin.*, *26*, 113–120.

Ben Othman, D., W. M. White, and J. Patchett (1989), The geochemistry of marine sediments, island arc magma genesis, and crust-mantle recycling, Earth Planet, *Sci. Lett.*, *94*, 1–21, doi:10.1016/0012-821X(89)90079-4.

Berggren, W. A., D. V. Kent, C. C. Swisher, M. P. Aubry (1995), Revised Cenozoic geochronology and chronostratigraphy, in *Geochronology, Time Scales and Global Stratigraphic Correlation*, edited by W. A. Berggren et al., *Spec. Publ. SEPM Soc. Sediment. Geol.*, *54*, 129-212.

Bodet, F., and U. Schärer (2001), Pb isotope systematics and time-integrated Th/U of SE-Asian continental crust recorded by single K-feldspar grains in large rivers, *Chem. Geol.*, *177*, 265–285, doi:10.1016/S0009-2541(00)00413-7.

Brookfield, M. E. (1998), The evolution of the great river systems of southern Asia during the Cenozoic India-Asia collision: Rivers draining southwards, *Geomorphology*, *22*, 285–312, doi:10.1016/S0169-555X(97)00082-2.

Carter, A., D. Roques, C. Bristow, and P. D. Kinny (2001), Understanding Mesozoic accretion in southeast Asia: Significance of Triassic thermotectonism (Indosinian orogeny) in Vietnam, *Geology*, *29*, 211–214, doi:10.1130/0091-7613(2001)029<0211:UMAISA>2.0.CO;2.

Castillo, P. R., J. H. Natland, Y. Niu, and P. F. Lonsdale (1998), Sr, Nd and Pb isotopic variation along the Pacific-Antarctic risecrest, 53–57°S: Implications for the composition and dynamics of the South Pacific upper mantle, Earth Planet, *Sci. Lett.*, *154*, 109–125, doi:10.1016/S0012-821X(97)00172-6.

Chen, J., and B.-M. Jahn (1998), Crustal evolution of southeastern China: Nd and Sr isotopic evidence, *Tectonophysics*, *284*, 101–133, doi:10.1016/S0040-1951(97)00186-8.

Chen, Z., et al. (1999), GPS monitoring of the crustal motion in southwestern China, *Chin. Sci. Bull.*, *44*, 1804–1807.

Clark, M. K., L. M. Schoenbohm, L. H. Royden, K. X. Whipple, B. C. Burchfiel, X. Zhang, W. Tang, E. Wang, and L. Chen (2004), Surface uplift, tectonics, and erosion of eastern Tibet from large-scale drainage patterns, *Tectonics*, *23*, TC1006, doi.10.1029/2002TC001402.

Clark, M. K., et al. (2005), Late Cenozoic uplift of southeastern Tibet, *Geology*, *33*, 525–528, doi:10.1130/G21265.1.

Clift, P. D., et al. (2002), Nd and Pb isotope variability in the Indus River system: Implications for sediment provenance and crustal heterogeneity in the western Himalaya, *Earth Planet. Sci. Lett.*, *200*, 91–106, doi:10.1016/S0012-821X(02)00620-9.

Clift, P. D., G. D. Layne, and J. Blusztajn (2004), Marine sedimentary evidence for monsoon strengthening, Tibetan uplift and drainage evolution in east Asia, in *Continent-Ocean Interactions in the East Asian Marginal Seas, Geophys. Monogr. Ser*, vol. 149, edited by P. Clift et al., pp. 255–282, AGU, Washington, D. C.

Clift, P. D., J. Blusztajn, and A. D. Nguyen (2006a), Large-scale drainage capture and surface uplift in eastern Tibet–SW China before 24 Ma inferred from sediments of the Hanoi Basin, Vietnam, *Geophys. Res. Lett.*, *33*, L19403, doi:10.1029/2006GL027772.

Clift, P. D., A. Carter, I. H. Campbell, M. S. Pringle, N. Van Lap, C. M. Allen, K. V. Hodges, and M. T. Tan (2006b), Thermochronology of mineral grains in the Red and Mekong Rivers, Vietnam: Provenance and exhumation implications for Southeast Asia, *Geochem. Geophys. Geosyst.*, *7*, Q10005, doi:10.1029/2006GC001336.

Colin, C., L. Turpin, J. Bertaux, A. Desprairies, and C. Kissel (1999), Erosional history of the Himalayan and Burman ranges during the last two glacial-interglacial cycles, Earth Planet, *Sci. Lett.*, *171*, 647–660, doi:10.1016/S0012-821X(99)00184-3.

Darbyshire, D. P. F., and R. J. Sewell (1997), Nd and Sr isotope geochemistry of plutonic rocks from Hong Kong: Implications for granite petrogenesis, regional structure and crustal evolution, *Chem. Geol.*, *143*, 81–93, doi:10.1016/S0009-2541(97)00101-0.

DePaolo, D. J., and G. J. Wasserburg (1976), Nd isotopic variations and petrogenetic models, *Geophys. Res. Lett.*, *3*, 249–252, doi:10.1029/GL003i005p00249.

Derry, L. A., and C. France-Lanord (1996), Neogene Himalayan weathering history and river $^{87}Sr/^{86}Sr$: Impact on the marine Sr record, *Earth Planet. Sci. Lett.*, *142*, 59–74, doi:10.1016/0012-821X(96)00091-X.

Galer, S. J. H. (1986), *Chemical and Isotopic Studies of Crust-Mantle Differentiation and the Generation of Mantle Heterogeneity*, 278 pp., Univ. of Cambridge, Cambridge, U. K.

Gariepy, C., C. J. Allègre, and R. H. Xu (1985), The Pb-isotope geochemistry of granitoids from the Himalaya-Tibet collision zone: Implications for crustal evolution, *Earth Planet. Sci. Lett.*, *74*, 220–234, doi:10.1016/0012-821X(85)90023-8.

Garzione, C. N., J. Quade, P. G. DeCelles, and N. B. English (2000), Predicting paleoelevation of Tibet and the Himalaya from $\delta^{18}O$ vs. altitude gradients in meteoric water across the Nepal Himalaya, *Earth Planet. Sci. Lett.*, *183*, 215–229, doi:10.1016/S0012-821X(00)00252-1.

Gilder, S. A., et al. (1996), Isotopic and paleomagnetic constraints on the Mesozoic tectonic evolution of south China, *J. Geophys. Res.*, *101*, 16,137–16,155, doi:10.1029/96JB00662.

Goldstein, S. L., and P. J. Hamilton (1984), A Sm-Nd isotopic study of atmospheric dusts and particulates from major river systems*Earth Planet. Sci. Lett.*, *70*, 221–236, doi:10.1016/0012-821X(84)90007-4.

Govindaraju, K. (1994), Compilation of working values and sample description for 383 geostandards, *Geostand. Newsl.*, *18*, 1–158.

Hall, R. (2002), Cenozoic geological and plate tectonic evolution of SE Asia and the SW Pacific: Computer-based reconstructions and animations, J, *Asian Earth Sci.*, *20*, 353–434, doi:10.1016/S1367-9120(01)00069-4.

Hamilton, P. J., R. K. Onions, D. Bridgwater, and A. Nutman (1983), Sm-Nd studies of Archean metasediments and metavolcanics from west Greenland and their implications for the Earth's early history, *Earth Planet. Sci. Lett.*, *62*, 263–272, doi:10.1016/0012-821X(83)90089-4.

Hannigan, R. E., and A. R. Basu (1998), Late diagenetic trace element remobilization in organic-rich black shales of the Taconic foreland basin of Quebec, Ontario and New York, in *Shales and Mudstones II*, edited by J. Schieber et al., pp. 209–234, Schweizerbart'sche, Zurich.

Hemming, S. R., et al. (1998), Provenance of Heinrich layers in Core V28-82, northeastern Atlantic: $^{40}Ar/^{39}Ar$ ages of ice-rafted hornblende, Pb isotopes in feldspar grains, and Nd-Sr-Pb isotopes in the fine sediment fraction, *Earth Planet. Sci. Lett.*, *164*, 317–333, doi:10.1016/S0012-821X(98)00224-6.

Huang, M., R. Maas, I. S. Buick, and I. S. Williams (2003a), Crustal response to continental collisions between the Tibet, Indian, South China and North China blocks: Geochronological constraints from the Songpan-Garze orogenic belt, western China, *J. Metamorph. Geol.*, *21*, 223–240.

Huang, M. H., I. S. Buick, and L. W. Hou (2003b), Tectonometamorphic evolution of the eastern Tibet Plateau: Evidence from the central Songpan-Garze orogenic belt, western China, *J. Petrol.*, *44*, 255–278, doi:10.1093/petrology/44.2.255.

Kapp, P., et al. (2000), Blueschist-bearing metamorphic core complexes in the Qiangtang Block reveal deep crustal structure of northern Tibet, *Geology*, *28*, 19–22, doi:10.1130/0091-7613(2000)28<19:BMCCIT>2.0.CO;2.

Lan, C.-Y., et al. (2003), Geochemical and Sr-Nd isotopic constraints from the Kontum massif, central Vietnam on the crustal evolution of the Indochina block, *Precambrian Res.*, *122*, 7–27, doi:10.1016/S0301-9268(02)00205-X.

Layne, G. D., and N. Shimizu (1998), Measurement of lead isotope ratios in common silicate and sulfide phases using the Cameca 1270 Ion Microprobe, in *Secondary Ion Mass Spectrometry SIMS XI*, edited by G. Gillen, pp. 63–65, John Wiley, New York.

Lepvrier, C., et al. (2004), The Early Triassic Indosinian orogeny in Vietnam (Truong Son Belt and Kontum Massif): Implications for the geodynamic evolution of Indochina, *Tectonophysics*, *393*, 87–118, doi:10.1016/j.tecto.2004.07.030.

Li, C., and A. Zheng (1993), Paleozoic stratigraphy in the Qiangtang region of Tibet: Relations of the Gondwana and Yangtze continents and ocean closure near the end of the Carboniferous, *Int. Geol. Rev.*, *35*, 797–804.

Li, Z.-X., X. Li, H. Zhou, and P. D. Kinny (2002), Grenvillian continental collision in South China: New SHRIMP U-Pb zircon results and implications for the configuration of Rodinia, *Geology*, *30*, 163–166, doi:10.1130/0091-7613(2002)030<3C0163:3AGCCISC>2.0.CO;2.

Li, X., et al. (2003), Geochemical and Nd isotopic variations in sediments of the South China Sea: A response to Cenozoic tectonism in SE Asia, Earth Planet, *Sci. Lett.*, *211*, 207–220, doi:10.1016/S0012-821X(03)00229-2.

Li, C., Z.-H. He, and Z.-M. Lui (2004), U-Pb and Sm-Nd dating of mafic dike swarms in southern Qiangtang, Qinghai-Tibet Plateau and its tectonic significance, *Geol. China*, *31*, 384–389.

Liu, Z., C. Colin, W. Huang, K. P. Le, S. Tong, Z. Chen, and A. Trentesaux (2007), Climatic and tectonic controls on weathering in south China and Indochina Peninsula: Clay mineralogical and geochemical investigations from the Pearl, Red, and Mekong drainage basins, *Geochem. Geophys. Geosyst.*, *8*, Q05005, doi:10.1029/2006GC001490.

Ma, C., C. Ehlers, C. Xu, Z. Li, and K. Yang (2000), The roots of the Dabieshan ultrahigh-pressure metamorphic terrane; constraints from geochemistry and Nd-Sr isotope systematics, *Precambrian Res.*, *102*, 279–301, doi:10.1016/S0301-9268(00)00069-3.

Mahoney, J., A. P. le Roex, Z. Peng, R. L. Fisher, and J. H. Natland (1992), Southwestern limits of Indian Ocean ridge mantle and the origin of low $^{206}Pb/^{204}Pb$ mid-ocean ridge basalt: Isotope systematics of the central Southwest Indian Ridge (17°–50°E), *J. Geophys. Res.*, *97*, 19,771–19,790, doi:10.1029/92JB01424.

Maluski, H., et al. (2001), Ar-Ar and fission-track ages in the Song Chay Massif: Early Triassic and Cenozoic tectonics in northern Vietnam, *J. Asian Earth Sci.*, *19*, 233–248, doi:10.1016/S1367-9120(00)00038-9.

McDaniel, D. K., S. R. Hemming, S. M. McLennan, and G. N. Hanson (1994), Petrographic, geochemical, and isotopic constraints on the provenance of the early Proterozoic Chelmsford Formation, Sudbury Basin, Ontario, *J. Sediment. Res. Sect. A*, *64*, 362–372.

Metcalfe, I. (1996), Pre-Cretaceous evolution of SE Asian terranes, in *Tectonic Evolution of SE Asia*, edited by R. Hall and D. J. Blundell, *Geol. Soc. Spec. Publ.*, *106*, 97-122.

Molnar, P., P. England, and J. Martinod (1993), Mantle dynamics, uplift of the Tibetan Plateau, and the Indian Monsoon, *Rev. Geophys.*, *31*, 357–396, doi:10.1029/93RG02030.

Nesbitt, H. W., and G. M. Young (1982), Early Proterozoic climates and plate motions inferred from major element chemistry of lutites, *Nature*, *299*, 715–717, doi:10.1038/299715a0.

Prell, W. L., and J. E. Kutzbach (1992), Sensitivity of the Indian Monsoon to forcing parameters and implications for its evolution, *Nature*, *360*, 647–652, doi:10.1038/360647a0.

Reichen, L. E., and J. J. Fahey (1962), An improved method for the determination of FeO in rocks and minerals including garnet, *U.S. Geol. Surv. Bull.*, *1144B*, 1–5.

Reid, A. J., C. J. L. Wilson, D. Phillips, and S. Liu (2005), Mesozoic cooling across the Yidun Arc, central-eastern Tibetan Plateau: A reconnaissance $^{40}Ar/^{39}Ar$ study, *Tectonophysics*, *398*, 45–66, doi:10.1016/j.tecto.2005.01.002.

Replumaz, A., and P. Tapponnier (2003), Reconstruction of the deformed collision zone Between India and Asia by back-

ward motion of lithospheric blocks, *J. Geophys. Res.*, *108*(B6), 2285, doi:10.1029/2001JB000661.

Replumaz, A., R. Lacassin, P. Tapponnier, and P. H. Leloup (2001), Large river offsets and Plio-Quaternary dextral slip rate on the Red River fault (Yunnan, China), *J. Geophys. Res.*, *106*, 819–836, doi:10.1029/2000JB900135.

Roger, F. (1994), Datation et tracage des granitodes associes a la chaine de Songpan-Garze (W. Sichuan, Chine) par les methods: U-Pb, Rb-Sr et Sm-Nd, Ph.D. thesis, 214 pp., Univ. Montpellier II, Montpellier, France.

Roger, F., et al. (1995), Miocene emplacement and deformation of the Konga Shan granite (Xianshui He fault zone, West Sichuan, China): Geodynamic implications, *Earth Planet. Sci. Lett.*, *130*, 201–216, doi:10.1016/0012-821X(94)00252-T.

Roger, F., N. Arnaud, S. Gilder, P. Tapponnier, M. Jolivet, M. Brunel, J. Malavieille, Z. Xu, and J. Yang (2003), Geochronological and geochemical constraints on Mesozoic suturing in east central Tibet, *Tectonics*, *22*(4), 1037, doi:10.1029/2002TC001466.

Ruhl, K. W., and K. V. Hodges (2005), The use of detrital mineral cooling ages to evaluate steady state assumptions in active orogens: An example from the central Nepalese Himalaya, *Tectonics*, *24*, TC4015, doi:10.1029/2004TC001712.

Schoenbohm, L. M., B. C. Burchfiel, and L. Chen (2006), Propagation of surface uplift, lower crustal flow, and Cenozoic tectonics of the southeast margin of the Tibetan Plateau, *Geology*, *34*, 813–816, doi:10.1130/G22679.1.

Singh, M., M. Sharma, and H. J. Tobschall (2005), Weathering of the Ganga alluvial plain, northern India: Implications from fluvial geochemistry of the Gomati River, *Appl. Geochem.*, *20*, 1–21, doi:10.1016/j.apgeochem.2004.07.005.

Spicer, R. A., et al. (2003), Constant elevation of southern Tibet over the past 15 million years, *Nature*, *421*, 622–624, doi:10.1038/nature01356.

Sun, S. S. (1980), Lead isotopic study of young volcanic rocks from mid-ocean ridges, ocean islands and island arcs, *Philos. Trans. R. Soc. London, Ser. A*, *297*, 409–445.

Todt, W., R. A. Cliff, A. Hanser, and A. W. Hofmann (1996), Evaluation of a ^{202}Pb-^{205}Pb double spike for high-precision lead isotope analysis, in *Earth Processes: Reading the Isotopic Code, Geophys. Monogr. Ser*, vol. 95, edited by A. Basu and S. R. Hart, pp. 429–437, AGU, Washington, D. C.

Tyrrell, S., P. D. W. Haughton, J. S. Daly, T. F. Kokfelt, and D. Gagnevin (2006), The use of the common Pb isotope composition of detrital K-feldspar grains as a provenance tool and its application to Upper Carboniferous paleodrainage, northern England, *J. Sediment. Res.*, *76*, 324–345, doi:10.2110/jsr.2006.023.

Vidal, P., A. Cocherie, and P. Le Fort (1982), Geochemical investigations of the origin of the Manaslu leucogranite (Himalaya, Nepal), *Geochim. Cosmochim. Acta*, *46*, 2279–2292, doi:10.1016/0016-7037(82)90201-0.

Wang, P. (2004), Cenozoic deformation and the history of sea-land interactions in Asia, in *Continent-Ocean Interactions in the East Asian Marginal Seas*, *Geophys. Monogr. Ser.*, vol. 149, edited by P. Clift et al., pp. 1–22, AGU, Washington, D. C.

Wang, J., and Z. Ye (2006), Dynamic modeling for crustal deformation in China: Comparisons between the theoretical prediction and the recent GPS data, *Phys Earth Planet Inter*, *155*, 201–207, doi:10.1016/j.pepi.2005.11.003.

Weislogel, A. L., et al. (2006), Detrital zircon provenance of the Late Triassic Songpan-Ganzi complex: Sedimentary record of collision of the North and South China blocks, *Geology*, *34*, 97–100, doi:10.1130/G21929.1.

Yang, S., S. Y. Jiang, H. F. Ling, X. P. Xia, M. Sun, and D. J. Wang (2007), Sr-Nd isotopic compositions of the Changjiang sediments: Implications for tracing sediment sources, *Sci. China, Ser. D*, *50*, 1556–1565.

Zhou, D., and S. A. Graham (1996), Songpan-Ganzi Triassic flysch complex of the West Qinling Shan as a remnant ocean basin, in *The Tectonic Evolution of Asia*, edited by A. Yin and M. Harrison, pp. 281–299, Cambridge Univ. Press, Cambridge, U. K.